The $\bar{q}q\bar{s}Q$ (q=u, d; Q=c, b) tetraquark system in a chiral quark model*

Gang Yang (杨刚)[1†] Jialun Ping (平加伦)[2‡] Jorge Segovia[3§]

[1]Department of Physics, Zhejiang Normal University, Jinhua 321004, China
[2]Department of Physics and Jiangsu Key Laboratory for Numerical Simulation of Large Scale Complex Systems, Nanjing Normal University, Nanjing 210023, China
[3]Departamento de Sistemas Físicos, Químicos y Naturales, Universidad Pablo de Olavide, E-41013 Sevilla, Spain

Abstract: The S-wave $\bar{q}q\bar{s}Q$ ($q=u,d$; $Q=c,b$) tetraquarks, with spin-parities $J^P=0^+$, 1^+, and 2^+, in both isoscalar and isovector sectors, are systematically studied using a chiral quark model. The meson-meson, diquark-antidiquark, and K-type arrangements of quarks and all possible color wave functions are comprehensively considered. The four-body system is solved using the Gaussian expansion method, a highly efficient computational approach. Additonally, a complex-scaling formulation of the problem is established to disentangle bound, resonance, and scattering states. This theoretical framework has already been successfully applied in various tetra- and penta-quark systems. For the complete coupled channel and within the complex-range formulation, several narrow resonances of $\bar{q}q\bar{s}c$ and $\bar{q}q\bar{s}b$ systems are obtained, in each allowed $I(J^P)$-channel, within the energy regions of 2.4 – 3.4 GeV and 5.7 – 6.7 GeV, respectively. The predicted exotic states, which indicate a richer color structure when going towards multiquark systems beyond mesons and baryons, are expected to be confirmed in future high-energy particle and nuclear experiments.

Keywords: quantum chromodynamics, quark models

DOI: 10.1088/1674-1137/ad39cd

I. INTRODUCTION

In 2020, two charm-strange resonances, $X_0(2900)$ and $X_1(2900)$, which are presumably $ud\bar{s}\bar{c}$ tetraquark candidates, were reported by the LHCb collaboration for $B^+\to D^+D^-K^+$ decays [1, 2]. In 2023, this collaboration announced two new resonant states, $T^0_{c\bar{s}}(2900)$ and $T^{++}_{c\bar{s}}(2900)$, in a combined amplitude analysis of $B^0\to\bar{D}^0D^+_s\pi^-$ and $B^+\to D^-D^+_s\pi^+$ decays [3, 4]. These observations indicated that the signals may be open-charm tetraquark candidates with minimal quark content $c\bar{s}q\bar{q}$ ($q=u,d$). Without the ability to disentangle the masses and widths of these two resonances, the LHCb collaboration determined that they are $2.908\pm0.011\pm0.020$ GeV and $0.136\pm0.023\pm0.011$ GeV in both cases; moreover, their quantum numbers $I(J^P)$ were determined to be $1(0^+)$.

These observations have inspired numerous theoretical investigations. Generally, the $T_{c\bar{s}}(2900)$ states can be fully identified as a molecular structures in the $I(J^P)=1(0^+)$ channel using phenomenological models such as those presented in Refs. [5−9]. However, interpretations of compact configurations [10, 11], threshold effects [12], and triangle anomalies [13] have also been proposed through various effective field theory approaches and quark models based on the color flux-tube. Additionally, the strong decay properties [14−16] and production mechanisms [17−20] of the exotic states have been investigated. In addition, more $T_{c\bar{s}}$ resonances within an energy region of 2.1 – 3.0 GeV have been predicted theoretically [5, 7, 10].

In addition to the mentioned T_{cs} and $T_{c\bar{s}}$ states, dozens of exotic hadrons, whose masses are generally near the threshold of two conventional heavy flavored hadrons, have been reported experimentally within the last 20 years. Owing to the rate at which they were being

Received 10 January 2024; Accepted 2 April 2024; Published online 3 April 2024

* Partially supported by the National Natural Science Foundation of China (12305093, 11535005, 11775118), the Natural Science Foundation of Zhejiang Province, China(LQ22A050004), the Ministerio Español de Ciencia e Innovación (PID2019-107844GB-C22, PID2022-140440NB-C22), the Junta de Andalucía under contract Nos. Operativo FEDER Andalucía (2014-2020 UHU-1264517, P18-FR-5057 and also PAIDI FQM-370)

† E-mail: yanggang@zjnu.edu.cn
‡ E-mail: jlping@njnu.edu.cn
§ E-mail: jsegovia@upo.es

discovered, they have garnered considerable theoretical interest, and experiments through various approaches have been developed by theorists to reveal the nature of the unexpected exotic states, which are overall good candidates of multiquark systems. Particularly, many extensive reviews [21−38], which explain in detail particular theoretical methods and thus capture particular interpretations of exotic hadrons, can be found in the literature.

Herein, we comprehensively investigate $\bar{q}q\bar{s}Q$ ($q=u$, d; $Q=c,b$) tetraquark systems with spin-parities of $J^P=0^+$, 1^+, and 2^+ in the isospin $I=0$ and 1 sectors. A variational formalism based on a highly efficient numerical approach called the Gaussian expansion method (GEM) [39] is used to solve the four-body Hamiltonian, which is based on a chiral quark model that has been used to describe reasonably well various tetra- and penta-quark systems [40−49]. Moreover, bound, resonant, and scattering states can be fully disentangled by solving the complex scaled Schrödinger equation formulated using the complex scaling method (CSM). Furthermore, the meson-meson, diquark-antidiquark, and K-type arrangements of quarks, as well as their couplings with all possible color wave functions, are considered.

The remainder of this manuscript is organized as follows. Sec. II presents the theoretical framework and a brief description of the chiral quark model and $\bar{q}q\bar{s}Q$ tetraquark wave functions. Sec. III analyzes and discusses the calculated results. Finally, a summary is presented in Sec. IV.

II. THEORETICAL FRAMEWORK

Phenomenological models continue to be the main tools used to study the nature of multiquark candidates observed experimentally. Hence, $\bar{q}q\bar{s}Q$ tetraquark systems are systematically investigated using a chiral quark model. Moreover, a highly accurate computing approach for the few-body system, the GEM, and an effective CSM are adopted to investigate the bound, resonant, and scattering states of the multiquark system. The theoretical formalism employed herein is described in detail in Ref. [26], and we shall focus on the most relevant features of the model and the numerical approach for $\bar{q}q\bar{s}Q$ tetraquarks.

A. Hamiltonian

The four-body problem is studied using a complex scaled Schrödinger equation:

$$[H(\theta)-E(\theta)]\Psi_{JM}(\theta)=0, \tag{1}$$

where the general form of the four-body Hamiltonian for a QCD-inspired chiral quark model is expressed as

$$H(\theta)=\sum_{i=1}^{4}\left(m_i+\frac{\vec{p}_i^{\,2}}{2m_i}\right)-T_{\rm CM}+\sum_{j>i=1}^{4}V(\vec{r}_{ij}e^{i\theta}), \tag{2}$$

where m_i is the constituent quark mass, $\vec{p}_i$ is the momentum of a quark, $T_{\rm CM}$ is the center-of-mass kinetic energy, and the last term is the two-body potential. By introducing an artificial parameter in the Hamiltonian, called the rotated angle θ, we find three types of complex eigenvalues, *viz.* bound, resonance, and scattering states can be simultaneously studied. In particular, the bound and resonance states are independent of θ, with the former always placed on the real-axis of the complex energy plane, and the latter located above the threshold line with a total decay width of $\Gamma=-2\,{\rm Im}(E)$. Meanwhile, the energy dots corresponding to scattering states are unstable under rotations of θ and align along the threshold line, which also changes with θ.

The dynamics of $\bar{q}q\bar{s}Q$ tetraquark systems is driven by two-body complex scaled potentials:

$$V(\vec{r}_{ij}e^{i\theta})=V_\chi(\vec{r}_{ij}e^{i\theta})+V_{\rm CON}(\vec{r}_{ij}e^{i\theta})+V_{\rm OGE}(\vec{r}_{ij}e^{i\theta}). \tag{3}$$

In particular, dynamical chiral symmetry breaking, color-confinement, and perturbative one-gluon exchange interactions, which are considered the most relevant features of QCD at its low energy regime, are taken into account. Because the low-lying S-wave positive parity $\bar{q}q\bar{s}Q$ tetraquark states are investigated herein, only the central and spin-spin terms of the potential are considered.

A consequence of the dynamical breaking of chiral symmetry is that Goldstone boson exchange interactions appear between constituent light quarks u, d, and s. Thus, the complex scaled chiral interaction can be expressed as

$$V_\chi(\vec{r}_{ij}e^{i\theta})=V_\pi(\vec{r}_{ij}e^{i\theta})+V_\sigma(\vec{r}_{ij}e^{i\theta})+V_K(\vec{r}_{ij}e^{i\theta})+V_\eta(\vec{r}_{ij}e^{i\theta}), \tag{4}$$

where

$$V_\pi\left(\vec{r}_{ij}e^{i\theta}\right)=\frac{g_{ch}^2}{4\pi}\frac{m_\pi^2}{12m_im_j}\frac{\Lambda_\pi^2}{\Lambda_\pi^2-m_\pi^2}m_\pi\Big[Y(m_\pi r_{ij}e^{i\theta}) -\frac{\Lambda_\pi^3}{m_\pi^3}Y(\Lambda_\pi r_{ij}e^{i\theta})\Big](\vec{\sigma}_i\cdot\vec{\sigma}_j)\sum_{a=1}^{3}(\lambda_i^a\cdot\lambda_j^a), \tag{5}$$

$$V_\sigma\left(\vec{r}_{ij}e^{i\theta}\right)=-\frac{g_{ch}^2}{4\pi}\frac{\Lambda_\sigma^2}{\Lambda_\sigma^2-m_\sigma^2}m_\sigma\Big[Y(m_\sigma r_{ij}e^{i\theta}) -\frac{\Lambda_\sigma}{m_\sigma}Y(\Lambda_\sigma r_{ij}e^{i\theta})\Big], \tag{6}$$

$$V_K\left(\vec{r}_{ij}\mathrm{e}^{\mathrm{i}\theta}\right)=\frac{g_{ch}^2}{4\pi}\frac{m_K^2}{12m_im_j}\frac{\Lambda_K^2}{\Lambda_K^2-m_K^2}m_K\Big[Y(m_Kr_{ij}\mathrm{e}^{\mathrm{i}\theta})-\frac{\Lambda_K^3}{m_K^3}Y(\Lambda_Kr_{ij}\mathrm{e}^{\mathrm{i}\theta})\Big](\vec{\sigma}_i\cdot\vec{\sigma}_j)\sum_{a=4}^{7}(\lambda_i^a\cdot\lambda_j^a), \tag{7}$$

$$V_\eta\left(\vec{r}_{ij}\mathrm{e}^{\mathrm{i}\theta}\right)=\frac{g_{ch}^2}{4\pi}\frac{m_\eta^2}{12m_im_j}\frac{\Lambda_\eta^2}{\Lambda_\eta^2-m_\eta^2}m_\eta\Big[Y(m_\eta r_{ij}\mathrm{e}^{\mathrm{i}\theta})-\frac{\Lambda_\eta^3}{m_\eta^3}Y(\Lambda_\eta r_{ij}\mathrm{e}^{\mathrm{i}\theta})\Big](\vec{\sigma}_i\cdot\vec{\sigma}_j)\Big[\cos\theta_p\left(\lambda_i^8\cdot\lambda_j^8\right)-\sin\theta_p\Big], \tag{8}$$

where $Y(x)=\mathrm{e}^{-x}/x$ is the Yukawa function. The physical η meson, instead of the octet one, is considered by introducing a model parameter of angle θ_p. λ^a represents the $SU(3)$ flavor Gell-Mann matrices. Obtained from their experimental values, m_π, m_K, and m_η are the masses of the $SU(3)$ Goldstone bosons. The value of m_σ is determined through the relation $m_\sigma^2\simeq m_\pi^2+4m_{u,d}^2$ [50]. Finally, the chiral coupling constant, g_{ch}, is determined from the πNN coupling constant through

$$\frac{g_{ch}^2}{4\pi}=\frac{9}{25}\frac{g_{\pi NN}^2}{4\pi}\frac{m_{u,d}^2}{m_N^2}, \tag{9}$$

which assumes that flavor $SU(3)$ is an exact symmetry only broken by the different mass of the strange quark.

Color confinement should be encoded in the non-Abelian character of QCD. On one hand, lattice-regularized QCD has demonstrated that multi-gluon exchanges produce an attractive linearly increasing potential proportional to the distance between infinite-heavy quarks [51]. On the other hand, the spontaneous creation of light-quark pairs from the QCD vacuum may result, at the same scale, in a breakup of the created color flux-tube [51]. We can phenomenologically describe the above two observations as

$$V_{\mathrm{CON}}(\vec{r}_{ij}\mathrm{e}^{\mathrm{i}\theta})=\left[-a_c(1-\mathrm{e}^{-\mu_c r_{ij}\mathrm{e}^{\mathrm{i}\theta}})+\Delta\right](\lambda_i^c\cdot\lambda_j^c), \tag{10}$$

where λ^c denotes the $SU(3)$ color Gell-Mann matrices, and a_c, μ_c, and Δ are model parameters. When the rotated angle θ is 0°, the real-range potential in Eq. (10) is linear at short inter-quark distances with an effective confinement strength $\sigma=-a_c\mu_c(\lambda_i^c\cdot\lambda_j^c)$, whereas it becomes a constant at large distances, $V_{\mathrm{thr.}}=(\Delta-a_c)(\lambda_i^c\cdot\lambda_j^c)$.

Beyond the chiral symmetry breaking energy scale, we also expect the dynamics to be governed by perturbative effects of QCD. In particular, the one-gluon exchange potential, which includes the so-called Coulomb and color-magnetic interactions, is the leading order contribution:

$$V_{\mathrm{OGE}}(\vec{r}_{ij}\mathrm{e}^{\mathrm{i}\theta})=\frac{1}{4}\alpha_s(\lambda_i^c\cdot\lambda_j^c)\Big[\frac{1}{r_{ij}\mathrm{e}^{\mathrm{i}\theta}}-\frac{1}{6m_im_j}(\vec{\sigma}_i\cdot\vec{\sigma}_j)\frac{\mathrm{e}^{-r_{ij}\mathrm{e}^{\mathrm{i}\theta}/r_0(\mu_{ij})}}{r_{ij}\mathrm{e}^{\mathrm{i}\theta}r_0^2(\mu_{ij})}\Big], \tag{11}$$

where $\vec{\sigma}$ denotes the Pauli matrices, and $r_0(\mu_{ij})=\hat{r}_0/\mu_{ij}$ depends on the reduced mass of a $q\bar{q}$ pair. Moreover, the regularized contact term is

$$\delta(\vec{r}_{ij}\mathrm{e}^{\mathrm{i}\theta})\sim\frac{1}{4\pi r_0^2(\mu_{ij})}\frac{\mathrm{e}^{-r_{ij}\mathrm{e}^{\mathrm{i}\theta}/r_0(\mu_{ij})}}{r_{ij}\mathrm{e}^{\mathrm{i}\theta}}. \tag{12}$$

An effective scale-dependent strong coupling constant, $\alpha_s(\mu_{ij})$, provides a consistent description of mesons and baryons from light to heavy quark sectors. The frozen coupling constant is expressed as (for instance, Ref. [52])

$$\alpha_s(\mu_{ij})=\frac{\alpha_0}{\ln\left(\frac{\mu_{ij}^2+\mu_0^2}{\Lambda_0^2}\right)}, \tag{13}$$

where α_0, μ_0, and Λ_0 are model parameters.

All the discussed model parameters are summarized in Table 1. They have been fixed along the last two decades by thorough studies of hadron phenomenology such as meson [53−55] and baryon [56−58] spectra, hadron decays and reactions [59−61], the coupling between con-

Table 1. Chiral quark model parameters.

Quark masses	$m_q\,(q=u,d)$ /MeV	313
	m_s /MeV	555
	m_c /MeV	1752
	m_b /MeV	5100
Goldstone bosons	$\Lambda_\pi=\Lambda_\sigma$ /fm^{-1}	4.20
	$\Lambda_\eta=\Lambda_K$ fm^{-1}	5.20
	$g_{ch}^2/(4\pi)$	0.54
	$\theta_P(^\circ)$	-15
Confinement	a_c /MeV	430
	μ_c /fm^{-1}	0.70
	Δ /MeV	181.10
OGE	α_0	2.118
	Λ_0/fm^{-1}	0.113
	μ_0/MeV	36.976
	$\hat{r}_0$/MeV fm	28.17

ventional hadrons and hadron-hadron thresholds [62−64], and molecular hadron-hadron formation [65−67]. Furthermore, for a later discussion, Table 2 lists theoretical and experimental (if available) masses of $1S$ and $2S$ states of $q\bar{q}$ and $\bar{q}Q$ $(q=u,d,s;Q=c,b)$ mesons.

Table 2. Theoretical and experimental (if available) masses of $1S$ and $2S$ states of $q\bar{q}$ and $\bar{q}Q(q=u,d,s;Q=c,b)$ mesons (unit: MeV).

Meson	nL	$M_{\rm The.}$	$M_{\rm Exp.}$	Meson	nL	$M_{\rm The.}$	$M_{\rm Exp.}$
π	$1S$	149	140	η	$1S$	689	548
	$2S$	1291	1300		$2S$	1443	1295
ρ	$1S$	772	770	ω	$1S$	696	782
	$2S$	1479	1450		$2S$	1449	1420
K	$1S$	481	494	K^*	$1S$	907	892
	$2S$	1468	1460		$2S$	1621	1630
D	$1S$	1897	1870	D^*	$1S$	2017	2007
	$2S$	2648	–		$2S$	2704	–
D_s	$1S$	1989	1968	D_s^*	$1S$	2115	2112
	$2S$	2705	–		$2S$	2769	–
B	$1S$	5278	5280	B^*	$1S$	5319	5325
	$2S$	5984	–		$2S$	6005	–
B_s	$1S$	5355	5367	B_s^*	$1S$	5400	5415
	$2S$	6017	–		$2S$	6042	–

B. Wave function

The S-wave $\bar{q}q\bar{s}Q$ $(q=u,d;Q=c,b)$ tetraquark configurations are shown in Fig. 1. Figs. 1(a) and (b) show the meson-meson structures, Fig. 1(c) shows the diquark-antidiquark arrangement, and (d) to (f) show the K-type configurations. For solving a manageable4-body problem for fully-coupled channels, the K-type configurations are occasionally restricted, as in our previous investigations [41, 42]. Furthermore, only one configuration would be sufficient for the calculation if all radial and orbital excited states are considered; however, this is inefficient. Therefore, a more economic method to use is the combination of the different mentioned structures.

At the quark level, the total wave function of a tetraquark system is the internal product of color, spin, flavor, and space wave functions. First, regarding the color degree-of-freedom, the colorless wave function of a 4-quark system in meson-meson configuration can be obtained using either two coupled color-singlet clusters, $1\otimes1$:

$$\chi_1^c=\frac{1}{3}(\bar{r}r+\bar{g}g+\bar{b}b)\times(\bar{r}r+\bar{g}g+\bar{b}b), \tag{14}$$

or two coupled color-octet clusters, $8\otimes8$:

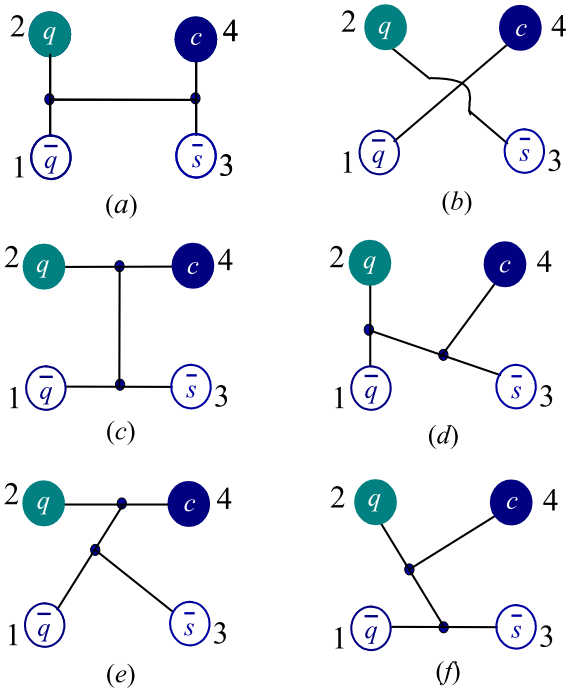

Fig. 1. (color online) Six types of configurations are considered for the $\bar{q}q\bar{s}Q$ $(q=u,d;Q=c,b)$ tetraquarks. Panels (a) and (b) are meson-meson structures, panel (c) is diquark-antidiquark arrangement, and the K-type configurations are shown in panels (d) to (f).

$$\begin{aligned}\chi_2^c=\frac{\sqrt{2}}{12}(&3\bar{b}r\bar{r}b+3\bar{g}r\bar{r}g+3\bar{b}g\bar{g}b+3\bar{g}b\bar{b}g+3\bar{r}g\bar{g}r\\&+3\bar{r}b\bar{b}r+2\bar{r}r\bar{r}r+2\bar{g}g\bar{g}g+2\bar{b}b\bar{b}b-\bar{r}r\bar{g}g\\&-\bar{g}g\bar{r}r-\bar{b}b\bar{g}g-\bar{b}b\bar{r}r-\bar{g}g\bar{b}b-\bar{r}r\bar{b}b).\end{aligned} \tag{15}$$

The first color state is the so-called color-singlet channel, and the second one is the named hidden-color channel.

The color wave functions associated to the diquark-antidiquark structure are the coupled color triplet-antitriplet clusters, $3\otimes\bar{3}$:

$$\begin{aligned}\chi_3^c=\frac{\sqrt{3}}{6}(&\bar{r}r\bar{g}g-\bar{g}r\bar{r}g+\bar{g}g\bar{r}r-\bar{r}g\bar{g}r+\bar{r}r\bar{b}b\\&-\bar{b}r\bar{r}b+\bar{b}b\bar{r}r-\bar{r}b\bar{b}r+\bar{g}g\bar{b}b-\bar{b}g\bar{g}b\\&+\bar{b}b\bar{g}g-\bar{g}b\bar{b}g),\end{aligned} \tag{16}$$

and the coupled color sextet-antisextet clusters, $6\otimes\bar{6}$:

$$\begin{aligned}\chi_4^c=\frac{\sqrt{6}}{12}(&2\bar{r}r\bar{r}r+2\bar{g}g\bar{g}g+2\bar{b}b\bar{b}b+\bar{r}r\bar{g}g+\bar{g}r\bar{r}g\\&+\bar{g}g\bar{r}r+\bar{r}g\bar{g}r+\bar{r}r\bar{b}b+\bar{b}r\bar{r}b+\bar{b}b\bar{r}r\\&+\bar{r}b\bar{b}r+\bar{g}g\bar{b}b+\bar{b}g\bar{g}b+\bar{b}b\bar{g}g+\bar{g}b\bar{b}g).\end{aligned} \tag{17}$$

Meanwhile, the possible color-singlet wave functions of three K-type structures are given by

$$\chi^c_5=\chi^c_2, \tag{18}$$

$$\chi^c_6=\chi^c_1, \tag{19}$$

$$\begin{aligned}\chi^c_7=&\frac{1}{2\sqrt{6}}(\bar{r}b\bar{b}r+\bar{r}r\bar{b}b+\bar{g}b\bar{b}g+\bar{g}g\bar{b}b+\bar{r}g\bar{g}r+\bar{r}r\bar{g}g\\&+\bar{b}b\bar{g}g+\bar{b}g\bar{g}b+\bar{g}g\bar{r}r+\bar{g}r\bar{r}g+\bar{b}b\bar{r}r+\bar{b}r\bar{r}b)\\&+\frac{1}{\sqrt{6}}(\bar{r}r\bar{r}r+\bar{g}g\bar{g}g+\bar{b}b\bar{b}b),\end{aligned} \tag{20}$$

$$\begin{aligned}\chi^c_8=&\frac{1}{2\sqrt{3}}(\bar{r}b\bar{b}r-\bar{r}r\bar{b}b+\bar{g}b\bar{b}g-\bar{g}g\bar{b}b+\bar{r}g\bar{g}r-\bar{r}r\bar{g}g\\&-\bar{b}b\bar{g}g+\bar{b}g\bar{g}b-\bar{g}g\bar{r}r+\bar{g}r\bar{r}g-\bar{b}b\bar{r}r+\bar{b}r\bar{r}b),\end{aligned} \tag{21}$$

$$\chi^c_9=\chi^c_7, \tag{22}$$

$$\chi^c_{10}=-\chi^c_8. \tag{23}$$

For the flavor degree-of-freedom, both iso-scalar $(I=0)$ and iso-vector $(I=1)$ channels of $\bar{q}q\bar{s}Q$ $(q=u,d;Q=c,b)$ tetraquarks should be considered. In particular, for meson-meson and part of K-type (Fig. 1(d) and (e)) configurations, the flavor wave functions, which are denoted as $\chi^{f_1}_{I,M_I}$, are

$$\chi^{f_1}_{0,0}=-\frac{1}{\sqrt{2}}(\bar{u}u\bar{s}Q+\bar{d}d\bar{s}Q), \tag{24}$$

$$\chi^{f_1}_{1,0}=\frac{1}{\sqrt{2}}(-\bar{u}u\bar{s}Q+\bar{d}d\bar{s}Q). \tag{25}$$

Additionally, using similar notations $\chi^{f_2}_{I,M_I}$ and $\chi^{f_3}_{I,M_I}$, where the superscripts 2 and 3 denote symmetry and anti-symmetry properties between the $\bar{q}\bar{s}$-pair, respectively, the wave functions of diquark-antidiquark and K-type (Fig. 1(f)) structures are given by

$$\chi^{f_2}_{0,0}=-\frac{1}{2}(\bar{u}u\bar{s}Q+\bar{s}u\bar{u}Q+\bar{d}d\bar{s}Q+\bar{s}d\bar{d}Q), \tag{26}$$

$$\chi^{f_3}_{0,0}=+\frac{1}{2}(-\bar{u}u\bar{s}Q+\bar{s}u\bar{u}Q-\bar{d}d\bar{s}Q+\bar{s}d\bar{d}Q), \tag{27}$$

$$\chi^{f_2}_{1,0}=+\frac{1}{2}(-\bar{u}u\bar{s}Q-\bar{s}u\bar{u}Q+\bar{d}d\bar{s}Q+\bar{s}d\bar{d}Q), \tag{28}$$

$$\chi^{f_3}_{1,0}=+\frac{1}{2}(-\bar{u}u\bar{s}Q+\bar{s}u\bar{u}Q+\bar{d}d\bar{s}Q-\bar{s}d\bar{d}Q). \tag{29}$$

Herein, the third component of the isospin, M_I, is fixed to zero for simplicity, and this is because there is no flavor-dependent interaction in the Hamiltonian that can distinguish the third component of the isospin I.

Now, let us consider the S-wave ground states with spin (S) ranging from 0 to 2. Therefore, the spin wave functions, $\chi^{\sigma_i}_{S,M_S}$, are given by (M_S can be set to be equal to S without losing generality):

$$\chi^{\sigma_{u_1}}_{0,0}(4)=\chi^{\sigma}_{00}\chi^{\sigma}_{00}, \tag{30}$$

$$\chi^{\sigma_{u_2}}_{0,0}(4)=\frac{1}{\sqrt{3}}(\chi^{\sigma}_{11}\chi^{\sigma}_{1,-1}-\chi^{\sigma}_{10}\chi^{\sigma}_{10}+\chi^{\sigma}_{1,-1}\chi^{\sigma}_{11}), \tag{31}$$

$$\begin{aligned}\chi^{\sigma_{u_3}}_{0,0}(4)=&\frac{1}{\sqrt{2}}\Big((\sqrt{\frac{2}{3}}\chi^{\sigma}_{11}\chi^{\sigma}_{\frac{1}{2},-\frac{1}{2}}-\sqrt{\frac{1}{3}}\chi^{\sigma}_{10}\chi^{\sigma}_{\frac{1}{2},\frac{1}{2}})\chi^{\sigma}_{\frac{1}{2},-\frac{1}{2}}\\&-(\sqrt{\frac{1}{3}}\chi^{\sigma}_{10}\chi^{\sigma}_{\frac{1}{2},-\frac{1}{2}}-\sqrt{\frac{2}{3}}\chi^{\sigma}_{1,-1}\chi^{\sigma}_{\frac{1}{2},\frac{1}{2}})\chi^{\sigma}_{\frac{1}{2},\frac{1}{2}}\Big),\end{aligned} \tag{32}$$

$$\chi^{\sigma_{u_4}}_{0,0}(4)=\frac{1}{\sqrt{2}}(\chi^{\sigma}_{00}\chi^{\sigma}_{\frac{1}{2},\frac{1}{2}}\chi^{\sigma}_{\frac{1}{2},-\frac{1}{2}}-\chi^{\sigma}_{00}\chi^{\sigma}_{\frac{1}{2},-\frac{1}{2}}\chi^{\sigma}_{\frac{1}{2},\frac{1}{2}}), \tag{33}$$

for $(S,M_S)=(0,0)$, by

$$\chi^{\sigma_{w_1}}_{1,1}(4)=\chi^{\sigma}_{00}\chi^{\sigma}_{11}, \tag{34}$$

$$\chi^{\sigma_{w_2}}_{1,1}(4)=\chi^{\sigma}_{11}\chi^{\sigma}_{00}, \tag{35}$$

$$\chi^{\sigma_{w_3}}_{1,1}(4)=\frac{1}{\sqrt{2}}(\chi^{\sigma}_{11}\chi^{\sigma}_{10}-\chi^{\sigma}_{10}\chi^{\sigma}_{11}), \tag{36}$$

$$\begin{aligned}\chi^{\sigma_{w_4}}_{1,1}(4)=&\sqrt{\frac{3}{4}}\chi^{\sigma}_{11}\chi^{\sigma}_{\frac{1}{2},\frac{1}{2}}\chi^{\sigma}_{\frac{1}{2},-\frac{1}{2}}-\sqrt{\frac{1}{12}}\chi^{\sigma}_{11}\chi^{\sigma}_{\frac{1}{2},-\frac{1}{2}}\chi^{\sigma}_{\frac{1}{2},\frac{1}{2}}\\&-\sqrt{\frac{1}{6}}\chi^{\sigma}_{10}\chi^{\sigma}_{\frac{1}{2},\frac{1}{2}}\chi^{\sigma}_{\frac{1}{2},\frac{1}{2}},\end{aligned} \tag{37}$$

$$\chi^{\sigma_{w_5}}_{1,1}(4)=(\sqrt{\frac{2}{3}}\chi^{\sigma}_{11}\chi^{\sigma}_{\frac{1}{2},-\frac{1}{2}}-\sqrt{\frac{1}{3}}\chi^{\sigma}_{10}\chi^{\sigma}_{\frac{1}{2},\frac{1}{2}})\chi^{\sigma}_{\frac{1}{2},\frac{1}{2}}, \tag{38}$$

$$\chi^{\sigma_{w_6}}_{1,1}(4)=\chi^{\sigma}_{00}\chi^{\sigma}_{\frac{1}{2},\frac{1}{2}}\chi^{\sigma}_{\frac{1}{2},\frac{1}{2}}, \tag{39}$$

for $(S,M_S)=(1,1)$, and by

$$\chi^{\sigma_1}_{2,2}(4)\quad=\chi^{\sigma}_{11}\chi^{\sigma}_{11}, \tag{40}$$

for $(S, M_S) = (2, 2)$. The superscripts $u_1, u_2, \ldots, u_4$ and $w_1, w_2, \ldots, w_6$ determine the spin wave function for each configuration of the $\bar{q}q\bar{s}Q$ tetraquark system, their values are listed in Table 3. Furthermore, the expressions above are obtained by considering the coupling between two sub-clusters whose spin wave functions are given by trivial $SU(2)$ algebra, and the necessary basis is expressed as

$$\chi^{\sigma}_{00} = \frac{1}{\sqrt{2}}(\chi^{\sigma}_{\frac{1}{2},\frac{1}{2}}\chi^{\sigma}_{\frac{1}{2},-\frac{1}{2}} - \chi^{\sigma}_{\frac{1}{2},-\frac{1}{2}}\chi^{\sigma}_{\frac{1}{2},\frac{1}{2}}), \tag{41}$$

$$\chi^{\sigma}_{11} = \chi^{\sigma}_{\frac{1}{2},\frac{1}{2}}\chi^{\sigma}_{\frac{1}{2},\frac{1}{2}}, \tag{42}$$

$$\chi^{\sigma}_{1,-1} = \chi^{\sigma}_{\frac{1}{2},-\frac{1}{2}}\chi^{\sigma}_{\frac{1}{2},-\frac{1}{2}}, \tag{43}$$

$$\chi^{\sigma}_{10} = \frac{1}{\sqrt{2}}(\chi^{\sigma}_{\frac{1}{2},\frac{1}{2}}\chi^{\sigma}_{\frac{1}{2},-\frac{1}{2}} + \chi^{\sigma}_{\frac{1}{2},-\frac{1}{2}}\chi^{\sigma}_{\frac{1}{2},\frac{1}{2}}). \tag{44}$$

The Rayleigh-Ritz variational principle, which is one of the most used tools to solve eigenvalue problems, is employed to solve the Schrödinger-like four-body system equation. Generally, within a complex-scaling theoretical framework, the spatial wave function is expressed as follows:

$$\psi_{LM_L} = \left[\left[\phi_{n_1 l_1}(\vec{\rho}\mathrm{e}^{\mathrm{i}\theta})\phi_{n_2 l_2}(\vec{\lambda}\mathrm{e}^{\mathrm{i}\theta})\right]_l \phi_{n_3 l_3}(\vec{R}\mathrm{e}^{\mathrm{i}\theta})\right]_{LM_L}, \tag{45}$$

where the internal Jacobi coordinates are defined as

$$\vec{\rho} = \vec{x}_1 - \vec{x}_{2(4)}, \tag{46}$$

Table 3. Values of the superscripts $u_1, \ldots, u_4$ and $w_1, \ldots, w_6$ that specify the spin wave function for each configuration of $\bar{q}q\bar{s}Q$ ($q = u, d$; $Q = c, b$) tetraquark systems.

	Di-meson	Diquark-antidiquark	K_1	K_2	K_3
u_1	1	3			
u_2	2	4			
u_3			5	7	9
u_4			6	8	10
w_1	1	4			
w_2	2	5			
w_3	3	6			
w_4			7	10	13
w_5			8	11	14
w_6			9	12	15

$$\vec{\lambda} = \vec{x}_3 - \vec{x}_{4(2)}, \tag{47}$$

$$\vec{R} = \frac{m_1\vec{x}_1 + m_{2(4)}\vec{x}_{2(4)}}{m_1 + m_{2(4)}} - \frac{m_3\vec{x}_3 + m_{4(2)}\vec{x}_{4(2)}}{m_3 + m_{4(2)}}, \tag{48}$$

for the meson-meson configurations of Figs. 1(a) and (b); and as

$$\vec{\rho} = \vec{x}_1 - \vec{x}_3, \tag{49}$$

$$\vec{\lambda} = \vec{x}_2 - \vec{x}_4, \tag{50}$$

$$\vec{R} = \frac{m_1\vec{x}_1 + m_3\vec{x}_3}{m_1 + m_3} - \frac{m_2\vec{x}_2 + m_4\vec{x}_4}{m_2 + m_4}, \tag{51}$$

for the diquark-antidiquark structure of Fig. 1(c). The remaining K-type configurations shown in Fig. 1(d) to (f) are (i, j, k, l take values according to panels (d) to (f) of Fig. 1):

$$\vec{\rho} = \vec{x}_i - \vec{x}_j, \tag{52}$$

$$\vec{\lambda} = \vec{x}_k - \frac{m_i\vec{x}_i + m_j\vec{x}_j}{m_i + m_j}, \tag{53}$$

$$\vec{R} = \vec{x}_l - \frac{m_i\vec{x}_i + m_j\vec{x}_j + m_k\vec{x}_k}{m_i + m_j + m_k}. \tag{54}$$

It is obvious now that the center-of-mass kinetic term T_{CM} can be completely eliminated for a non-relativistic system defined in any of the above sets of relative motion coordinates.

The basis expansion of the genuine wave function of Eq. (45) is a crucial aspect in the Rayleigh-Ritz variational method. By employing the GEM [39], which has proven to be efficient in solving the bound-state problem of multi-body systems, we expand all the spatial wave functions corresponding to the four relative motions with Gaussian basis functions, whose sizes are obtained using geometric progression. Hence, the form of orbital wave functions, ϕ, in Eq. (45) for a S-wave tetraquark system is simply expressed as

$$\phi_{nlm}(\vec{r}\mathrm{e}^{\mathrm{i}\theta}) = \sqrt{1/4\pi}\,N_{nl}\,(r\mathrm{e}^{\mathrm{i}\theta})^l\,\mathrm{e}^{-\nu_n(r\mathrm{e}^{\mathrm{i}\theta})^2}. \tag{55}$$

Finally, the complete wave function, which fulfills the Pauli principle, is written as

$$\Psi_{JM_J,I} = \sum_{i,j,k} c_{ijk}\Psi_{JM_J,I,i,j,k} = \sum_{i,j,k} c_{ijk}\mathcal{A}\left[\left[\psi_{LM_L}\chi^{\sigma_i}_{SM_S}(4)\right]_{JM_J}\chi^{f_j}_I\chi^c_k\right], \quad (56)$$

where $\mathcal{A}$ is the anti-symmetry operator of $\bar{q}q\bar{s}Q$ tetraquark systems, which considers the use of $SU(3)$ flavor symmetry. According to Fig. 1, it is defined as

$$\mathcal{A} = 1 - (13). \quad (57)$$

This is necessary in our theoretical framework because the complete wave function of the four-quark system is constructed from two sub-clusters: meson-meson, diquark-antidiquark, and K-type configurations.

Because the anti-symmetry operator and Gaussian basis functions are employed, the different channels, which include meson-meson in singlet- and hidden-color arrangements, diquark-antidiquark, and K-type configurations, are not orthogonal to each other. This is inevitable in our theoretical framework; however, the off-diagonal matrix elements are very small numerically and negligible compared with the diagonal ones. Accordingly, a quantitative analysis of the inter-quark distances,

$$r_{q\bar{q}} = \sqrt{\langle\Psi_{JM_J,I}|r^2_{q\bar{q}}|\Psi_{JM_J,I}\rangle}, \quad (58)$$

and a qualitative survey of dominant components,

$$C_p = \sum_{i,j,k\in C_p}\langle c^l_{ijk}\Psi_{JM_J,I,ijk}|c^r_{ijk}\Psi_{JM_J,I,ijk}\rangle, \quad (59)$$

can be conducted. In the formula above, c^l_{ijk} and c^r_{ijk} are the left and right generalized eigenvectors, respectively, of the complete anti-symmetric complex wave-function. Additionally, note that only the real part of these complex quantities are discussed herein to gain insights into the nature of $\bar{q}q\bar{s}Q$ tetraquarks.

In the next section, which discusses the computed results on the $\bar{q}q\bar{s}Q$ tetraquarks, we first study the systems through a real-range analysis, *viz.*, the rotated angle θ is equal to 0°. In this case, when a complete coupled-channel calculation of matrix diagonalization is performed, possible resonant states are embedded in the continuum. However, we can employ the CSM, with appropriate non-zero values of θ, to disentangle bound, resonance, and scattering states in a complex energy plane. Accordingly, for solving manageable eigevalue problems, the artificial parameter of rotated angle is ranged form 0° to 6°. Meanwhile, with the cooperation of real- and complex-range computations, available exotic states, which are first obtained within a complex-range analysis and then can be identified among continuum states according to its mass in a real-range calculation, are further investigated by analyzing their dominant quark arrangements, sizes, and decay patterns.

III. RESULTS

The S-wave $\bar{q}q\bar{s}Q$ $(q = u, d; Q = c, b)$ tetraquarks are systematically studied by including meson-meson, diquark-antidiquark, and K-type configurations. Therefore, the total angular momentum, J, coincides with the total spin, S, and can have values of 0, 1, and 2. Thus, the parity of tetraquark system is positive. Furthermore, both the iso-scalar $(I = 0)$ and -vector $(I = 1)$ sectors of $\bar{q}q\bar{s}Q$ tetraquarks are considered.

Tables 4 to 27 list the calculated results of low-lying $\bar{q}q\bar{s}Q$ tetraquark states. In particular, real-range computations on the lowest-lying masses of each tetraquark system in the allowed $I(J^P)$ quantum numbers are presented in Tables 4, 6, 8, 10, 12, 14, 16, 18, 20, 22, 24, and 26. Therein, the considered meson-meson, diquark-antidiquark, and K-type configurations are listed in the first column; if available, the experimental value of the non-interacting di-meson threshold is labeled in parentheses. In the second column, each channel is assigned with an index, which indicates a particular combination of spin $(\chi^{\sigma_i}_J)$, flavor $(\chi^{f_j}_I)$, and color (χ^c_k) wave functions, which are shown explicitly in the third column. The theoretical mass calculated in each channel is shown in the fourth column, and the coupled result for each type of configuration is presented in the last one. The last row of the table indicates the lowest-lying mass, which is obtained in a complete coupled-channel calculation within the real-range formalism.

In a further step, a complete coupled-channel calculation is performed using the CSM in each $I(J^P)$ $\bar{q}q\bar{s}Q$ tetraquark system. Figures 2 to 13 show the distribution of complex eigenenergies, and therein, the obtained resonance states are indicated inside circles. Several insights about the nature of these resonances are given by calculating their interquark sizes and dominant components; correspondingly, results are listed among Tables 5, 7, 9, 11, 13, 15, 17, 19, 21, 23, 25 and 27. In particular, because the $SU(3)$ flavor symmetry is considered for the $\bar{q}q\bar{s}Q$ tetraquark systems, four types of quark distances, which are $r_{q\bar{q}}$, $r_{\bar{q}\bar{q}}$, $r_{c\bar{q}}$, and r_{qc} $(q = u, d, s)$, are calculated. Finally, a summary of our most salient results is presented in Table 28.

To explain our delicate compromise between obtaining reliable results and reasonable times of computation, let us explain our method of obtaining results when we perform a fully-coupled channel computation using the CSM. First, the bound, resonance, and scattering states are complex values distributed in a two dimensional plane, we can observe in the figures below that rotations

from 0° to 6° enable us to reasonably distinguish all bound, resonance, and scattering states when the imaginary part of the complex energy is lower than ≈ 15 MeV. Second, regardless of how clear the figure may be, we follow the behavior of each energy point with respect to the rotated angle from zero to six degrees; thus, we can distinguish wether they belong to a particular meson-meson threshold or can be something else. In the second case, we perform some extra internal assessments before claiming that the state may be a resonance (there is no doubt when an energy point is a bound state because it is localized in the real axis and does not move with respect the angle). Third, we require a black-circle (2°), red triangle (4°), and blue square (6°) leaving the meson-meson lines and forming a cluster to attract our attention; subsequently, we make some extra assessments related with the evolution of the energy point with respect the theta parameter and its connection with the 0° case to finally claim that it is actually a resonance.

Now, we describe in detail our theoretical findings for each sector of $\bar{q}q\bar{s}Q$ tetraquarks.

A. $\bar{q}q\bar{s}c$ (q=u, d) tetraquarks

Several resonances whose masses range from 2.8 to 3.5 GeV are obtained in this tetraquark sector. Each isoscalar and -vector sectors with total spin and parity $J^P = 0^+$, 1^+, and 2^+ are discussed individually below.

The $I(J^P) = 0(0^+)$ sector: Four meson-meson configurations, ηD_s, ωD_s^*, KD and K^*D^* in both color-singlet and -octet channels, four diquark-antidiquark structures, along with three K-type configurations are individually calculated in Table 4. The lowest channel is the color-singlet state of KD, whose theoretical mass is 2378 MeV, the other three meson-meson configurations with the same color channel are in an energy region of 2.6 to 3.0 GeV. No bound state is found. Additionally, the single channel calculations are performed in each exotic structure. The hidden-color channels of di-meson configurations are generally located in the $3.1-3.3$ GeV interval. This result also holds for the diquark-antidiquark and K-type structures, although the lowest masses of $(qc)(\bar{q}\bar{s})$ and K_3-type channels are 2.9 GeV.

After partially coupled-channel computations are performed in six configurations listed in Table 4, only the scattering state of KD and several color resonances, which masses are in an energy region of $2.7-2.9$ GeV, are obtained. Meanwhile, the lowest-lying mass of 2378 MeV for a KD scattering state remains even in the complete coupled-channel calculation.

Figure 2 presents the distribution of complex energies for the $\bar{q}q\bar{s}c$ tetraquark in the $0(0^+)$ channel calculated using the CSM for fully coupled channels. In particular, within a mass region of 2.35 to 3.35 GeV, five scattering states that include the ground states of KD, ηD_s, ωD_s^*, K^*D^*, and the radial excitation of $K(1S)D(2S)$ are well presented. However, in addition to the vast majority of scattering dots, one stable resonance pole is found and circled. The mass and width are 3006 and 6.3 MeV, respectively.

Table 5 shows the compositeness of the resonance

Table 4. Lowest-lying $\bar{q}q\bar{s}c$ tetraquark states with $I(J^P) = 0(0^+)$ calculated within the real range formulation of the chiral quark model. The allowed meson-meson, diquark-antidiquark, and K-type configurations are listed in the first column; when possible, the experimental value of the non-interacting meson-meson threshold is labeled in parentheses. Each channel is assigned an index in the second column; it reflects a particular combination of spin ($\chi_J^{\sigma_i}$), flavor ($\chi_I^{f_j}$), and color (χ_k^c) wave functions, which are shown explicitly in the third column. The theoretical mass obtained in each channel is shown in the fourth column, and the coupled result for each type of configuration is presented in the fifth column. When a complete coupled-channel calculation is performed, the last row of the table indicates the calculated lowest-lying mass (unit: MeV).

Channel	Index	$\chi_J^{\sigma_i};\chi_I^{f_j};\chi_k^c$ $[i;j;k]$	M	Mixed
$(\eta D_s)^1(2516)$	1	[1; 1; 1]	2678	
$(\omega D_s^*)^1(2894)$	2	[2; 1; 1]	2811	
$(KD)^1(2364)$	3	[1; 1; 1]	2378	
$(K^*D^*)^1(2899)$	4	[2; 1; 1]	2924	2378
$(\eta D_s)^8$	5	[1; 1; 2]	3293	
$(\omega D_s^*)^8$	6	[2; 1; 2]	3107	
$(KD)^8$	7	[1; 1; 2]	3169	
$(K^*D^*)^8$	8	[2; 1; 2]	3186	2932
$(qc)(\bar{q}\bar{s})$	9	[3; 2; 4]	3188	
$(qc)(\bar{q}\bar{s})$	10	[3; 3; 3]	2913	
$(qc)^*(\bar{q}\bar{s})^*$	11	[4; 2; 3]	3186	
$(qc)^*(\bar{q}\bar{s})^*$	12	[4; 3; 4]	3074	2777
K_1	13	[5; 1; 5]	3102	
	14	[6; 1; 5]	3286	
	15	[5; 1; 6]	3066	
	16	[6; 1; 6]	3071	2961
K_2	17	[7; 1; 7]	3094	
	18	[8; 1; 7]	3228	
	19	[7; 1; 8]	3207	
	20	[8; 1; 8]	3080	2850
K_3	21	[9; 2; 10]	2920	
	22	[9; 3; 9]	3071	
	23	[10; 2; 9]	3190	
	24	[10; 3; 10]	2920	2723
Complete coupled-channels:				2378

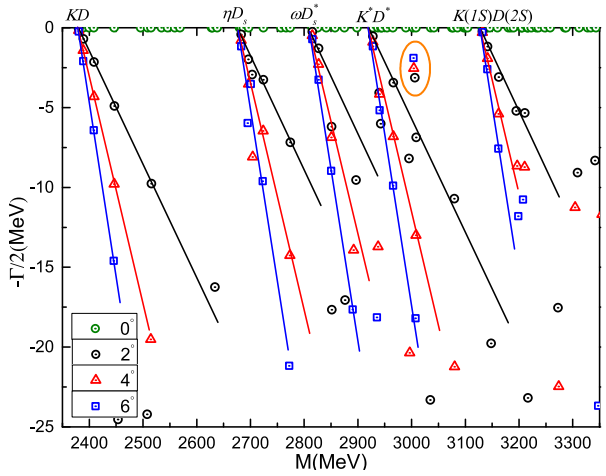

Fig. 2. (color online) Complete coupled-channel calculation of the $\bar{q}q\bar{s}c$ tetraquark system with $I(J^P) = 0(0^+)$ quantum numbers.

Table 5. Compositeness of the exotic resonance obtained in a complete coupled-channel calculation in the $0(0^+)$ state of the $\bar{q}q\bar{s}c$ tetraquark. In particular, the first column shows the resonance pole labeled by $M + \mathrm{i}\Gamma$ (unit: MeV); the second one shows the distance between any two quarks or quark-antiquark ($q = u, d, s$) pair (unit: fm) and the component of resonance state (S: di-meson structure in color-singlet channel; H: di-meson structure in the hidden-color channel; Di: diquark-antiquark configuration; K: K-type configuration).

Resonance	Structure
$3006 + \mathrm{i}6.3$	$r_{q\bar{q}}$: 1.64; $r_{\bar{q}\bar{q}}$: 2.23; $r_{c\bar{q}}$: 1.70; r_{qc} : 2.19
	S: 21.3%; H: 9.1%; Di: 13.1%; K: 56.5%

state. First, it is a loosely-bound structure with quark-antiquark distances of ~ 1.6 and ~ 2.2 fm for the qc and $\bar{q}\bar{q}$ pairs, respectively. Moreover, a strong coupling exists among singlet-, hidden-color, diquark-antidiquark, and K-type channels. The golden decays for this resonance are ωD_s^* and K^*D^*, which are the dominant components (21.3%) of the color-singlet channels.

The $I(J^P) = 0(1^+)$ sector: 36 channels contribute to this case, and results in real-range calculations are listed in Table 6. First, the lowest mass, 2498 MeV, in a single channel computation is the theoretical threshold value of KD^*. The other di-meson channels, which include ηD_s^*, $\omega D_s^{(*)}$, and $K^*D^{(*)}$, are generally located in $2.7 - 2.9$ GeV. All these states have a scattering nature. Six channels are also included in each exotic configuration. By referencing the calculated data on each channel, we find that the lowest masses in the hidden-color, diquark-antidiquark, and K-type configurations are all within $3.0 - 3.3$ GeV. Furthermore, color resonances with structures of diquark-antidiquark and K_3-type are still obtained at approximately 2.95 GeV.

In a further step, the lowest coupled-channel masses

Table 6. Lowest-lying $\bar{q}q\bar{s}c$ tetraquark states with $I(J^P) = 0(1^+)$ calculated within the real range formulation of the chiral quark model. The results are presented in the same manner as that in Table 4 (unit: MeV).

Channel	Index	$\chi_J^{\sigma_i}; \chi_I^{f_j}; \chi_k^c$ $[i; j; k]$	M	Mixed
$(\eta D_s^*)^1(2660)$	1	[1; 1; 1]	2804	
$(\omega D_s)^1(2750)$	2	[2; 1; 1]	2685	
$(\omega D_s^*)^1(2894)$	3	[3; 1; 1]	2811	
$(KD^*)^1(2501)$	4	[1; 1; 1]	2498	
$(K^*D)^1(2762)$	5	[2; 1; 1]	2804	
$(K^*D^*)^1(2899)$	6	[3; 1; 1]	2924	2498
$(\eta D_s^*)^8$	7	[1; 1; 2]	3296	
$(\omega D_s)^8$	8	[2; 1; 2]	3179	
$(\omega D_s^*)^8$	9	[3; 1; 2]	3147	
$(KD^*)^8$	10	[1; 1; 2]	3174	
$(K^*D)^8$	11	[2; 1; 2]	3191	
$(K^*D^*)^8$	12	[3; 1; 2]	3192	2897
$(qc)(\bar{q}\bar{s})^*$	13	[4; 2; 4]	3181	
$(qc)(\bar{q}\bar{s})^*$	14	[4; 3; 3]	2949	
$(qc)^*(\bar{q}\bar{s})$	15	[5; 2; 3]	3159	
$(qc)^*(\bar{q}\bar{s})$	16	[5; 3; 4]	3162	
$(qc)^*(\bar{q}\bar{s})^*$	17	[6; 2; 3]	3169	
$(qc)^*(\bar{q}\bar{s})^*$	18	[6; 3; 4]	3094	2852
K_1	19	[7; 1; 5]	3178	
	20	[8; 1; 5]	3121	
	21	[9; 1; 5]	3291	
	22	[7; 1; 6]	3044	
	23	[8; 1; 6]	3053	
	24	[9; 1; 6]	3113	3005
K_2	25	[10; 1; 7]	3109	
	26	[11; 1; 7]	3186	
	27	[12; 1; 7]	3187	
	28	[10; 1; 8]	3045	
	29	[11; 1; 8]	3213	
	30	[12; 1; 8]	3187	2956
K_3	31	[13; 2; 10]	3085	
	32	[13; 3; 9]	3083	
	33	[14; 2; 10]	3196	
	34	[14; 3; 9]	3112	
	35	[15; 2; 10]	3178	
	36	[15; 3; 9]	2946	2787
Complete coupled-channels:				2498

within each considered configuration are 2.50, 2.90, 2.85, 3.00, 2.96, and 2.79 GeV, respectively. These results indicate that the coupling effect is significantly weak in color-singlet channels, but it becomes stronger in other configurations. However, the bound state is still unavailable even in a complete coupled-channel scenario.

To find a possible resonance state in an excited energy region of 2.5 – 3.4 GeV, the fully coupled-channel calculation is further performed using the CSM, and results are plotted in a complex energy plane in Fig. 3. Therein, seven meson-meson scattering states are generally presented. They are ground states of $K^{(*)}D^{(*)}$, $\omega D_s^{(*)}$, and ηD_s^* and the first radial excited state of $K(1S)D^*(2S)$. However, three stable poles are obtained within the radial excited energy region, and their complex energies are $3119+\mathrm{i}19.8$, $3292+\mathrm{i}13.1$, and $3346+\mathrm{i}22$ MeV, respectively.

Table 7 shows particular features of the three resonances. First, their dominant components are all of exotic color structure, *i.e.*, the hidden-color, diquark-antidiquark, and K-type configurations. Moreover, the coupling among these three sectors is strong. The color resonances are also confirmed by calculating their sizes, with internal quark distances of about 1.1 – 1.7 fm. These resonances are expected to be experimentally studied in the $K^{(*)}D^{(*)}$ golden decay channels.

The $I(J^P)=0(2^+)$ state: Two meson-meson channels, ωD_s^* and K^*D^*, should be considered in the highest spin state. Table 8 shows that their lowest masses are simply the theoretical threshold values; hence, no bound state is found. Meanwhile, ten other channels of exotic structures are generally located in a mass region of 3.1 – 3.2 GeV. When coupled-channel calculations are performed in each specific configuration, color resonances are located at ~ 3.1 GeV, and the scattering state of ωD_s^*, which is the lowest-lying channel, remains at 2.8 GeV. This extremely weak coupling effect also holds for the complete coupled-channel study.

Nevertheless, three narrow resonances are obtained in a complex analysis on the fully coupled-channel computation. Figure 4 shows the two scattering states of ωD_s^* and K^*D^* within 2.8 – 3.4 GeV. Moreover, three stable poles against the descending cut lines occur when the rotated angle is varied from 0° to 6°.

The naturalness of these narrow resonances can be inferred from Table 9. In particular, the complex energies of these resonances are $2965+\mathrm{i}0.5$, $3026+\mathrm{i}3.8$, and $3344+\mathrm{i}3.3$ MeV, respectively. Compact structures are dominant when referring to their interquark sizes, which are about 1.4 fm. Furthermore, strong couplings exist among the color-singlet, hidden-color, diquark-antidiquark, and K-type configurations of these states. Because the singlet-color component are (~ 7%) of ωD_s^* and K^*D^* for these resonances, they can be experimentally in-

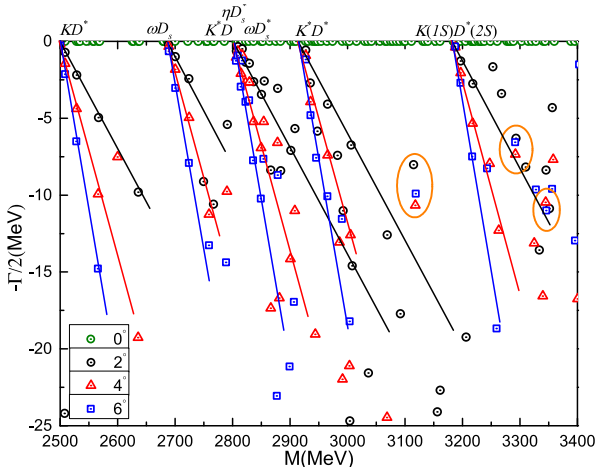

Fig. 3. (color online) Complete coupled-channel calculation of the $\bar{q}q\bar{s}c$ tetraquark system with $I(J^P)=0(1^+)$.

Table 7. Compositeness of exotic resonances obtained in a complete coupled-channel calculation in the $0(1^+)$ state of the $\bar{q}q\bar{s}c$ tetraquark. The results are presented in the same manner as that in Table 5.

Resonance	Structure
$3119+\mathrm{i}19.8$	$r_{q\bar{q}}$: 1.41; $r_{\bar{q}\bar{q}}$: 1.63; $r_{c\bar{q}}$: 1.03; r_{qc} : 1.61
	S: 8.5%; H: 18.7%; Di: 29.6%; K: 43.2%
$3292+\mathrm{i}13.1$	$r_{q\bar{q}}$: 1.14; $r_{\bar{q}\bar{q}}$: 1.13; $r_{c\bar{q}}$: 1.14; r_{qc} : 1.37
	S: 9.6%; H: 13.9%; Di: 34.5%; K: 42.0%
$3346+\mathrm{i}22.0$	$r_{q\bar{q}}$: 1.54; $r_{\bar{q}\bar{q}}$: 1.75; $r_{c\bar{q}}$: 1.49; r_{qc} : 1.64
	S: 6.7%; H: 8.8%; Di: 34.7%; K: 49.8%

Table 8. Lowest-lying $\bar{q}q\bar{s}c$ tetraquark states with $I(J^P)=0(2^+)$ calculated within the real range formulation of the chiral quark model. The results are presented in the same manner as that in Table 4 (unit: MeV).

Channel	Index	$\chi_J^{\sigma_i}$; $\chi_I^{f_j}$; χ_k^c $[i;j;k]$	M	Mixed
$(\omega D_s^*)^1(2894)$	1	[1; 1; 1]	2811	
$(K^*D^*)^1(2899)$	2	[1; 1; 1]	2924	2811
$(\omega D_s^*)^8$	3	[1; 1; 2]	3216	
$(K^*D^*)^8$	4	[1; 1; 2]	3201	3104
$(qc)^*(\bar{q}\bar{s})^*$	5	[1; 2; 3]	3132	
$(qc)^*(\bar{q}\bar{s})^*$	6	[1; 3; 4]	3130	3119
K_1	7	[1; 1; 5]	3200	
	8	[1; 1; 6]	3071	3070
K_2	9	[1; 1; 7]	3156	
	10	[1; 1; 8]	3159	3115
K_3	11	[1; 2; 10]	3119	
	12	[1; 3; 9]	3111	3104
Complete coupled-channels:				2811

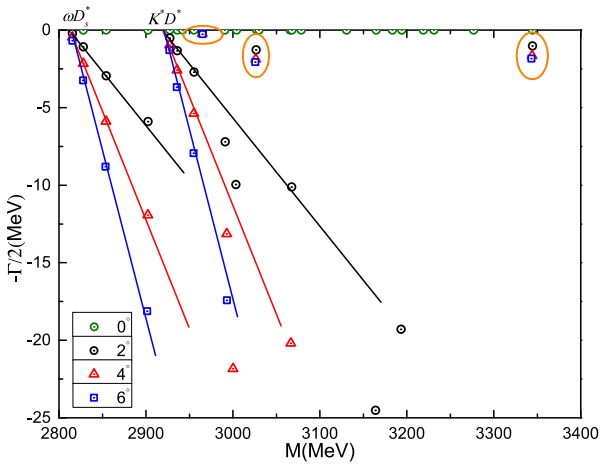

Fig. 4. (color online) Complete coupled-channel calculation of the $\bar{q}q\bar{s}c$ tetraquark system with $I(J^P) = 0(2^+)$ quantum numbers.

vestigated in any of the mentioned two-body strong decay processes.

The $I(J^P) = 1(0^+)$ sector: This case is similar to the $0(0^+)$ channel, *i.e.,* 24 channels are investigated, as shown in Table 10. First, πD_s, ρD_s^*, KD, and K^*D^* channels in both singlet- and hidden-color configurations are calculated. The lowest-lying state is the πD_s scattering state with a theoretical threshold value of 2138 MeV. Moreover, the other three meson-meson structures in color-singlet channels are also unbound, and the four hidden-color channels are generally located at 3.17 GeV. For the single channel computations of diquark-antidiquark and K-type configurations, the lowest masses are generally distributed within an energy region of $2.9-3.2$ GeV, except for a K_1-type channel with mass at 2475 MeV.

We do not find bound states when partially and fully coupled-channel calculations, in the real-range approximation, are performed. The complete coupled-channels study, in the complex range formulation, delivers six continuum states of πD_s, $K^{(*)}D^{(*)}$, ρD_s^*, $\pi(1S)D_s(2S)$, and $K(1S)D(2S)$, which are clearly presented in the $2.1-3.2$ GeV energy region of Fig. 5. Additionally, one stable resonance is obtained and circled in Fig. 5; its complex energy is predicted to be $2.8+\mathrm{i}0.002$ GeV. This state should be tentatively assigned to the experimentally observed $T_{c\bar{s}}(2900)$ state [3, 4]; however, its theoretical width is smaller than the experimental one. Thus, we cannot be optimistic in the assignment. Note that only two-body strong decay processes are considered, and the other channels not considered herein must contribute to its total decay width.

Table 11 lists the interquark distances and wavefunction components of the predicted exotic resonance. Its size is approximately 1.6 fm, and a strong coupling exists among the four considered configurations, *i.e.*, the color-singlet, hidden-color, diquark-antidiquark, and K-type structures. The color-singlet channels of πD_s and KD are comparable (~8%); hence, they are suggested to

Table 9. Compositeness of exotic resonances obtained in a complete coupled-channel calculation in the $0(2^+)$ state of the $\bar{q}q\bar{s}c$ tetraquark. The results are presented in the same manner as that in Table 5.

Resonance	Structure
$2965+\mathrm{i}0.5$	$r_{q\bar{q}}$: 1.18; $r_{\bar{q}\bar{q}}$: 1.19; $r_{c\bar{q}}$: 0.86; r_{qc} : 1.11
	S: 18.9%; H: 8.1%; Di: 27.8%; K: 45.2%
$3026+\mathrm{i}3.8$	$r_{q\bar{q}}$: 1.40; $r_{\bar{q}\bar{q}}$: 1.50; $r_{c\bar{q}}$: 1.02; r_{qc} : 1.43
	S: 15.4%; H: 12.6%; Di: 7.3%; K: 64.7%
$3344+\mathrm{i}3.3$	$r_{q\bar{q}}$: 1.46; $r_{\bar{q}\bar{q}}$: 1.54; $r_{c\bar{q}}$: 1.38; r_{qc} : 1.46
	S: 13.4%; H: 20.2%; Di: 18.5%; K: 47.9%

Table 10. Lowest-lying $\bar{q}q\bar{s}c$ tetraquark states with $I(J^P) = 1(0^+)$ calculated within the real range formulation of the chiral quark model. The results are presented in the same manner as that in Table 4 (unit: MeV).

Channel	Index	$\chi_J^{\sigma_i}; \chi_I^{f_j}; \chi_k^c$ $[i;j;k]$	M	Mixed
$(\pi D_s)^1(2108)$	1	[1; 1; 1]	2138	
$(\rho D_s^*)^1(2882)$	2	[2; 1; 1]	2887	
$(KD)^1(2364)$	3	[1; 1; 1]	2378	
$(K^*D^*)^1(2899)$	4	[2; 1; 1]	2924	2138
$(\pi D_s)^8$	5	[1; 1; 2]	3177	
$(\rho D_s^*)^8$	6	[2; 1; 2]	3167	
$(KD)^8$	7	[1; 1; 2]	3169	
$(K^*D^*)^8$	8	[2; 1; 2]	3105	2894
$(qc)(\bar{q}\bar{s})$	9	[3; 2; 4]	3188	
$(qc)(\bar{q}\bar{s})$	10	[3; 3; 3]	2913	
$(qc)^*(\bar{q}\bar{s})^*$	11	[4; 2; 3]	3084	
$(qc)^*(\bar{q}\bar{s})^*$	12	[4; 3; 4]	2956	2772
K_1	13	[5; 1; 5]	3166	
	14	[6; 1; 5]	3167	
	15	[5; 1; 6]	3157	
	16	[6; 1; 6]	2475	2460
K_2	17	[7; 1; 7]	2972	
	18	[8; 1; 7]	3228	
	19	[7; 1; 8]	3105	
	20	[8; 1; 8]	3080	2826
K_3	21	[9; 2; 10]	3062	
	22	[9; 3; 9]	2891	
	23	[10; 2; 9]	3190	
	24	[10; 3; 10]	2920	2700
Complete coupled-channels:				2138

be the golden decay channels.

The $I(J^P) = 1(1^+)$ sector: Among the six channels of the considered $\bar{q}q\bar{s}c$ tetraquark configurations, which include singlet-, hidden- color, diquark-antidiquark, and K-type structures, the lowest-lying state is the πD_s^* scattering state with a theoretical threshold at 2264 MeV. Meanwhile, this unbound nature remains unchanged in coupled-channel computations. The other five di-meson configurations in the color-singlet channels, which are $\rho D_s^{(*)}$ and $K^{(*)}D^{(*)}$, are also unbound. The masses of exotic color channels are generally located in the energy region of $2.9-3.2$ GeV, except for a K_1-type channel whose calculated mass is 2518 MeV. When coupled-channel calculations are performed in each of these structures, the lowest masses of hidden-color, diquark-antidiquark, K_1, K_2, and K_3 channels are 2951, 2871, 2509, 2972, and 2791 MeV, respectively. Although bound states are unavailable, the mentioned excited states obtained in each exotic color configuration may be good candidates of color resonances for the $\bar{q}q\bar{s}c$ tetraquark system.

Furthermore, Fig. 6 shows the distribution of complex energies in the fully coupled-channel calculation using the CSM. In particular, the top panel presents six scattering states, which have been discussed above. Within$2.25-3.15$ GeV, two stable poles are obtained, and they are indicated within circles. The lower resonance pole is

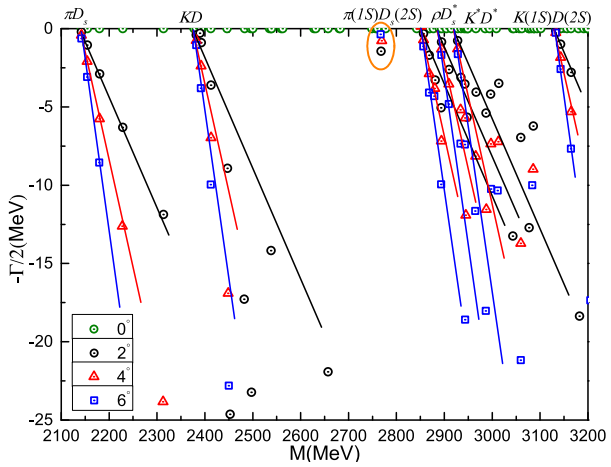

Fig. 5. (color online) Complete coupled-channel calculation of the $\bar{q}q\bar{s}c$ tetraquark system with $I(J^P) = 1(0^+)$ quantum numbers.

Table 11. Compositeness of the exotic resonance obtained in a complete coupled-channel calculation in the $1(0^+)$ state of the $\bar{q}q\bar{s}c$ tetraquark. The results are presented in the same manner as that in Table 5.

Resonance	Structure
$2770+i1.5$	$r_{q\bar{q}}: 1.05$; $r_{\bar{q}\bar{q}}: 1.80$; $r_{c\bar{q}}: 1.59$; $r_{qc}: 1.75$
	S: 15.6%; H: 19.2%; Di: 30.3%; K: 34.9%

Table 12. Lowest-lying $\bar{q}q\bar{s}c$ tetraquark states with $I(J^P) = 1(1^+)$ calculated within the real range formulation of the chiral quark model. The results are presented in the same manner as that in Table 4 (unit: MeV).

Channel	Index	$\chi_J^{\sigma_i}; \chi_I^{f_j}; \chi_k^c$ $[i;j;k]$	M	Mixed
$(\pi D_s^*)^1(2252)$	1	[1; 1; 1]	2264	
$(\rho D_s)^1(2738)$	2	[2; 1; 1]	2761	
$(\rho D_s^*)^1(2882)$	3	[3; 1; 1]	2887	
$(KD^*)^1(2501)$	4	[1; 1; 1]	2498	
$(K^*D)^1(2762)$	5	[2; 1; 1]	2804	
$(K^*D^*)^1(2899)$	6	[3; 1; 1]	2924	2264
$(\pi D_s^*)^8$	7	[1; 1; 2]	3181	
$(\rho D_s)^8$	8	[2; 1; 2]	3231	
$(\rho D_s^*)^8$	9	[3; 1; 2]	3203	
$(KD^*)^8$	10	[1; 1; 2]	3174	
$(K^*D)^8$	11	[2; 1; 2]	3191	
$(K^*D^*)^8$	12	[3; 1; 2]	3153	2951
$(qc)(\bar{q}\bar{s})^*$	13	[4; 2; 4]	3181	
$(qc)(\bar{q}\bar{s})^*$	14	[4; 3; 3]	2949	
$(qc)^*(\bar{q}\bar{s})$	15	[5; 2; 3]	3159	
$(qc)^*(\bar{q}\bar{s})$	16	[5; 3; 4]	3162	
$(qc)^*(\bar{q}\bar{s})^*$	17	[6; 2; 3]	3119	
$(qc)^*(\bar{q}\bar{s})^*$	18	[6; 3; 4]	3041	2871
K_1	19	[7; 1; 5]	3233	
	20	[8; 1; 5]	3183	
	21	[9; 1; 5]	3173	
	22	[7; 1; 6]	3134	
	23	[8; 1; 6]	3144	
	24	[9; 1; 6]	2518	2509
K_2	25	[10; 1; 7]	3158	
	26	[11; 1; 7]	3081	
	27	[12; 1; 7]	3187	
	28	[10; 1; 8]	3105	
	29	[11; 1; 8]	3110	
	30	[12; 1; 8]	3187	2972
K_3	31	[13; 2; 10]	3149	
	32	[13; 3; 9]	3148	
	33	[14; 2; 10]	3069	
	34	[14; 3; 9]	2942	
	35	[15; 2; 10]	3178	
	36	[15; 3; 9]	2946	2791
Complete coupled-channels:				2264

at $2470+\mathrm{i}1$ MeV, whereas the higher one is at $3134+\mathrm{i}2$ MeV. Finally, the bottom panel of Fig. 6 is an enlarged part of $2.85-3.00$ GeV. Therein, no stable resonance is found, and only three scattering states of ρD_s^*, $\pi(1S)$ $D_s^*(2S)$, and K^*D^* are presented.

Some insights into the nature of the narrow resonances can be found in Table 13. In particular, a compact $\bar{q}q\bar{s}c$ tetraquark structure is predicted for the lower resonance, and its size is about 0.9 fm. The coupling is strong among color-singlet (27%), diquark-antidiquark (14%), and K-type (56%) channels. Moreover, the dominant meson-meson decay channel is πD_s^*, which is expected to be confirmed in future experiments. In contrast, the higher resonance is a loosely-bound structure with a size of ~ 1.8 fm. The ratios between the components are similar to those at a lower resonance. This suggests that this state should be further studied using high energy experiments in the πD_s^* and K^*D^* decay channels.

The $I(J^P) = 1(2^+)$ sector: Twelve channels are considered in the highest spin and isospin tetraquark state, and our results are listed in Table 14. First, the bound states are not found in either single-channel or coupled-channel cases. The lowest channel is ρD_s^* with a theoretical threshold value of 2887 MeV, and another di-meson structure K^*D^* in the color-singlet channel is at 2924 MeV. The masses of other channels with exotic configurations are generally in an energy region of $3.1-3.2$ GeV, and each of the lowest coupled mass in one specific structure is ~ 3.16 GeV.

The complete coupled-channel calculation using CSM is shown in Fig. 7. In particular, two scattering states of ρD_s^* and K^*D^* are well presented within $2.8-3.5$ GeV. However, four stable poles occur above the threshold lines. Table 15 shows the resonance masses, widths, and wavefunction configurations. Moreover, we can infer the compact tetraquark structure, with a size of approximately $1.0-1.6$ fm, for the four resonances at $3031+\mathrm{i}0.7$, $3105+\mathrm{i}3.7$, $3373+\mathrm{i}4.2$, and $3455+\mathrm{i}12.9$ MeV, respectively. Additionally, strong couplings exist among the

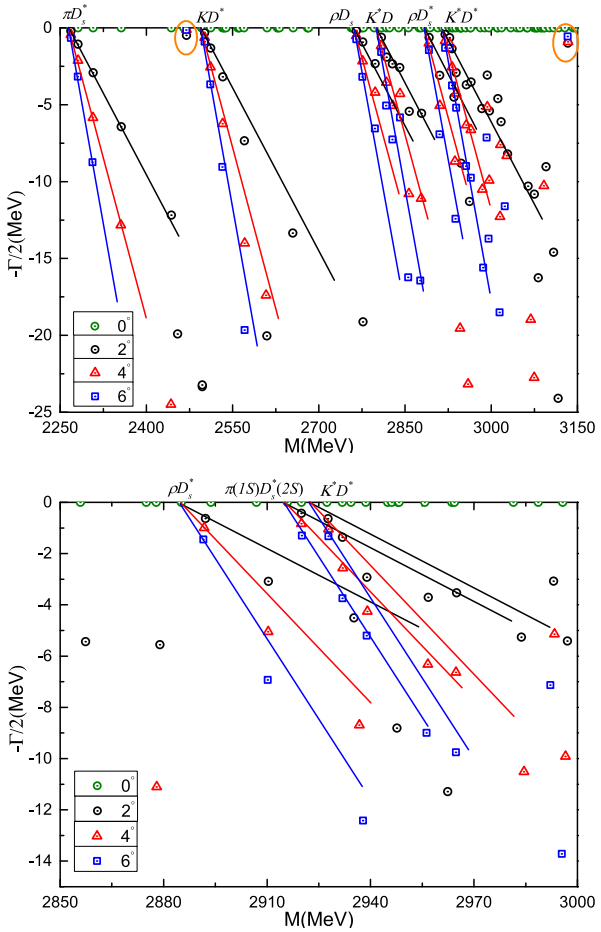

Fig. 6. (color online) Complete coupled-channel calculation of the $\bar{q}q\bar{s}c$ tetraquark system with $I(J^P) = 1(1^+)$ quantum numbers. In particular, the bottom panel shows enlarged parts of dense energy region from 2.85 GeV to 3.00 GeV.

Table 13. Compositeness of exotic resonances obtained in a complete coupled-channel calculation in the $1(1^+)$ state of the $\bar{q}q\bar{s}c$ tetraquark. The results are presented in the same manner as that in Table 5.

Resonance	Structure
$2470+\mathrm{i}1.0$	$r_{q\bar{q}}: 0.92$; $r_{\bar{q}\bar{q}}: 0.95$; $r_{c\bar{q}}: 0.88$; $r_{qc}: 0.79$
	S: 26.5%; H: 4.0%; Di: 13.5%; K: 56.0%
$3134+\mathrm{i}2.0$	$r_{q\bar{q}}: 1.79$; $r_{\bar{q}\bar{q}}: 1.87$; $r_{c\bar{q}}: 1.92$; $r_{qc}: 1.61$
	S: 16.1%; H: 18.0%; Di: 16.6%; K: 49.3%

Table 14. Lowest-lying $\bar{q}q\bar{s}c$ tetraquark states with $I(J^P) = 1(2^+)$ calculated within the real range formulation of the chiral quark model. The results are presented in the same manner as that in Table 4 (unit: MeV).

Channel	Index	$\chi_J^{\sigma_i}; \chi_I^{f_j}; \chi_k^c$ $[i;j;k]$	M	Mixed
$(\rho D_s^*)^1(2882)$	1	[1; 1; 1]	2887	
$(K^*D^*)^1(2899)$	2	[1; 1; 1]	2924	2887
$(\rho D_s^*)^8$	3	[1; 1; 2]	3265	
$(K^*D^*)^8$	4	[1; 1; 2]	3235	3140
$(qc)^*(\bar{q}\bar{s})^*$	5	[1; 2; 3]	3181	
$(qc)^*(\bar{q}\bar{s})^*$	6	[1; 3; 4]	3174	3166
K_1	7	[1; 1; 5]	3253	
	8	[1; 1; 6]	3161	3160
K_2	9	[1; 1; 7]	3202	
	10	[1; 1; 8]	3210	3166
K_3	11	[1; 2; 10]	3180	
	12	[1; 3; 9]	3174	3167
Complete coupled-channels:				2887

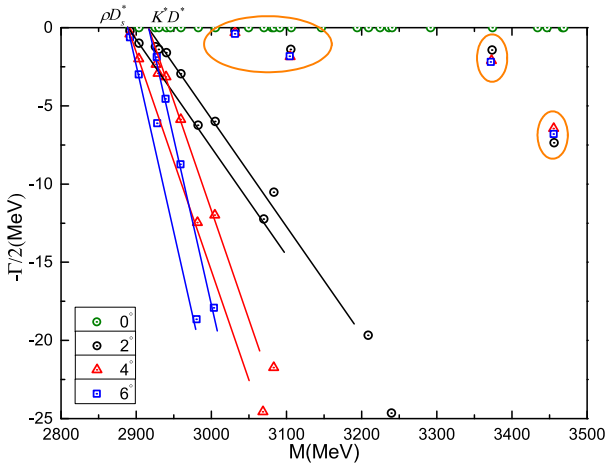

Fig. 7. (color online) Complete coupled-channel calculation of the $\bar{q}q\bar{s}c$ tetraquark system with $I(J^P) = 1(2^+)$ quantum numbers.

Table 15. Compositeness of exotic resonances obtained in a complete coupled-channel calculation in the $1(2^+)$ state of $\bar{q}q\bar{s}c$ tetraquark. The results are presented in the same manner as that in Table 5.

Resonance	Structure
$3031+i0.7$	$r_{q\bar{q}}$: 1.02; $r_{\bar{q}\bar{q}}$: 1.07; $r_{c\bar{q}}$: 0.94; r_{qc} : 1.00
	S: 16.4%; *H*: 14.1%; *Di*: 27.0%; *K*: 42.5%
$3105+i3.7$	$r_{q\bar{q}}$: 1.26; $r_{\bar{q}\bar{q}}$: 1.33; $r_{c\bar{q}}$: 0.99; r_{qc} : 1.26
	S: 4.0%; *H*: 21.6%; *Di*: 28.0%; *K*: 46.4%
$3373+i4.2$	$r_{q\bar{q}}$: 1.51; $r_{\bar{q}\bar{q}}$: 1.61; $r_{c\bar{q}}$: 1.45; r_{qc} : 1.55
	S: 8.0%; *H*: 10.6%; *Di*: 26.7%; *K*: 54.7%
$3455+i12.9$	$r_{q\bar{q}}$: 1.68; $r_{\bar{q}\bar{q}}$: 1.54; $r_{c\bar{q}}$: 1.30; r_{qc} : 1.45
	S: 6.6%; *H*: 9.8%; *Di*: 39.4%; *K*: 44.2%

singlet-, hidden-color, diquark-antidiquark, and *K*-type channels for these resonances. Both ρD_s^* and K^*D^* appear to be golden decay channels.

B. $\bar{q}q\bar{s}b$ tetraquarks

Three spin-parity states, $J^P = 0^+$, 1^+, and 2^+, with isospins of $I = 0$ and 1, are investigated for the $\bar{q}q\bar{s}b$ tetraquark system. Several narrow resonances are obtained in each $I(J^P)$ quantum number. The details of the calculation and the related discussion are presented in the following.

The $I(J^P) = 0(0^+)$ sector: Table 16 shows that 24 channels are investigated in this case. First, concerning the four color-singlet channels, which include ηB_s, ωB_s^*, KB, and K^*B^*, the lowest mass is 5759 MeV. This is the theoretical threshold value of KB, and the other channels are also unbound. Furthermore, the lowest-lying channels of hidden-color, diquark-antidiquark, and *K*-type configurations are generally located in a mass region of

Table 16. Lowest-lying $\bar{q}q\bar{s}b$ tetraquark states with $I(J^P) = 0(0^+)$ calculated within the real range formulation of the chiral quark model. The results are presented in the same manner as that in Table 4 (unit: MeV).

Channel	Index	$\chi_J^{\sigma_i}; \chi_I^{f_j}; \chi_k^c$ $[i;j;k]$	*M*	Mixed
$(\eta B_s)^1(5915)$	1	[1; 1; 1]	6044	
$(\omega B_s^*)^1(6197)$	2	[2; 1; 1]	6096	
$(KB)^1(5774)$	3	[1; 1; 1]	5759	
$(K^*B^*)^1(6217)$	4	[2; 1; 1]	6226	5759
$(\eta B_s)^8$	5	[1; 1; 2]	6613	
$(\omega B_s^*)^8$	6	[2; 1; 2]	6440	
$(KB)^8$	7	[1; 1; 2]	6361	
$(K^*B^*)^8$	8	[2; 1; 2]	6498	6292
$(qb)(\bar{q}\bar{s})$	9	[3; 2; 4]	6501	
$(qb)(\bar{q}\bar{s})$	10	[3; 3; 3]	6226	
$(qb)^*(\bar{q}\bar{s})^*$	11	[4; 2; 3]	6486	
$(qb)^*(\bar{q}\bar{s})^*$	12	[4; 3; 4]	6414	6113
K_1	13	[5; 1; 5]	6403	
	14	[6; 1; 5]	6585	
	15	[5; 1; 6]	6358	
	16	[6; 1; 6]	6387	6281
K_2	17	[7; 1; 7]	6427	
	18	[8; 1; 7]	6531	
	19	[7; 1; 8]	6520	
	20	[8; 1; 8]	6411	6210
K_3	21	[9; 2; 10]	6485	
	22	[9; 3; 9]	6382	
	23	[10; 2; 9]	6478	
	24	[10; 3; 10]	6221	6038
Complete coupled-channels:				5759

6.2 – 6.6 GeV. When coupled-channel computations are performed for each type of structure, the scattering nature of KB channel in di-meson structure is still obtained. Moreover, possible color resonances in K_3 and diquark-antidiquark structures are obtained at 6.04 and 6.11 GeV, respectively. The lowest masses of other three configurations are ~ 6.2 GeV. Finally, in a real-range computation, which is performed by including all of the above channels, the lowest mass of the $\bar{q}q\bar{s}b$ tetraquark system remains at the KB theoretical threshold, 5759 MeV.

In the next step, the complete coupled-channel case is studied in a complex-range formulation. Figure 8 shows the distribution of complex energies within 5.7 – 6.7 GeV. In particular, five scattering states, which are the ground states of KB, ηB_s, ωB_s^*, and K^*B^*, and the first radial excitation of $K(1S)B(2S)$, are well presented. Nevertheless,

five resonances are also found and circled in Fig. 8; their complex energies are $6011+\mathrm{i}9$, $6323+\mathrm{i}4$, $6397+\mathrm{i}13.8$, $6643+\mathrm{i}23.4$, and $6678+\mathrm{i}16$ MeV, respectively.

The details of the properties of such resonances are listed in Table 17. First, strong couplings exist among the singlet-, hidden-color, diquark-antidiquark, and K-type channels. Second, their sizes are less than 1.9 fm. In particular, the two lower resonances have sizes within $1.1-1.5$ fm, and the other three are extended to approximately $1.3-1.8$ fm. Third, for the lowest resonance at 6.0 GeV, the golden decay channel is the KB channel; the ωB_s^* and K^*B^* channels are dominant meson-meson components for the two resonances at 6.3 GeV, whereas the remaining two resonances at 6.6 GeV can be confirmed in KB and K^*B^* channels.

The $I(J^P) = 0(1^+)$ sector: Table 18 summarizes our results in the real-range formalism. First, the ηB_s^*, $\omega B_s^{(*)}$, and $K^{(*)}B^{(*)}$ channels in both color-singlet and -octet cases are considered. The lowest mass is 5.8 GeV, which is the KB^* theoretical threshold value. Moreover, no bound states in the other meson-meson channels are found, and the six hidden-color channels are generally located within the energy range of $6.3-6.6$ GeV. This energy region is also shared by the diquark-antidiquark and three K-type channels. In partially coupled-channel calculations, the coupling effect is weak in singlet- and hidden-color channels, their lowest masses are 5.80 and 6.32 GeV, respectively. Therefore, the bound state is still unavailable. Although strong couplings exist in diquark-antidiquark and three K-type channels, and the mass shift for the lowest-lying channel is $50-170$ MeV, the bound state is again not obtained. This result also holds for the fully coupled-channel calculation.

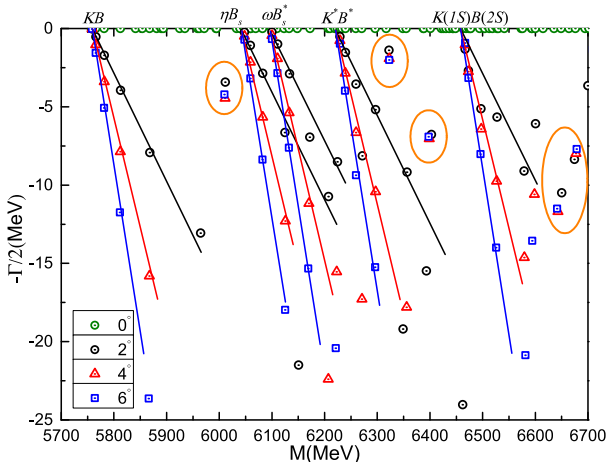

Fig. 8. (color online) Complete coupled-channel calculation of the $\bar{q}q\bar{s}b$ tetraquark system with $I(J^P) = 0(0^+)$ quantum numbers.

Table 17. Compositeness of exotic resonances obtained in a complete coupled-channel calculation in the $0(0^+)$ state of the $\bar{q}q\bar{s}b$ tetraquark. The results are presented in the same manner as that in Table 5.

Resonance	Structure
$6011+\mathrm{i}9.0$	$r_{q\bar{q}}$: 1.54; $r_{\bar{q}\bar{q}}$: 1.53; $r_{b\bar{q}}$: 0.66; r_{qb} : 1.48
	S: 19.5%; H: 7.5%; Di: 14.4%; K: 58.6%
$6323+\mathrm{i}4.0$	$r_{q\bar{q}}$: 1.16; $r_{\bar{q}\bar{q}}$: 1.24; $r_{b\bar{q}}$: 0.94; r_{qb} : 1.18
	S: 16.9%; H: 7.6%; Di: 21.9%; K: 53.6%
$6397+\mathrm{i}13.8$	$r_{q\bar{q}}$: 0.96; $r_{\bar{q}\bar{q}}$: 1.81; $r_{b\bar{q}}$: 1.74; r_{qb} : 1.76
	S: 7.8%; H: 17.6%; Di: 25.4%; K: 49.2%
$6643+\mathrm{i}23.4$	$r_{q\bar{q}}$: 1.35; $r_{\bar{q}\bar{q}}$: 1.61; $r_{b\bar{q}}$: 1.31; r_{qb} : 1.52
	S: 13.1%; H: 21.4%; Di: 31.1%; K: 34.4%
$6678+\mathrm{i}16.0$	$r_{q\bar{q}}$: 1.54; $r_{\bar{q}\bar{q}}$: 1.60; $r_{b\bar{q}}$: 1.33; r_{qb} : 1.52
	S: 17.9%; H: 27.8%; Di: 21.2%; K: 33.1%

In a further complex analysis of the complete coupled-channel, five resonances are obtained, and they are indicated in Fig. 9. We can observe, in addition to the seven scattering states of $K^{(*)}B^{(*)}$, $\omega B_s^{(*)}$, and ηB_s^* in the energy region of $5.8-6.7$ GeV, the five stable poles circled, with complex energies given by $6031+\mathrm{i}12$, $6298+\mathrm{i}16$, $6413+\mathrm{i}20.6$, $6607+\mathrm{i}4.2$, and $6652+\mathrm{i}7.7$ MeV, respectively.

Table 19 lists the calculated properties of the resonances to elucidate their nature. First, the strong coupling effects of different tetraquark configurations are reflected. Meanwhile, these resonances have sizes of about $1.6-1.9$ fm, except for the one at 6.4 GeV, whose size is less than 1.6 fm. Finally, the lowest resonance at 6.03 GeV is suggested to be experimentally studied in the KB^* decay channel. The K^*B and K^*B^* are dominant two-body strong decay channels for the 6.29 and 6.41 GeV resonances, whereas the KB^* is the golden channel for the remaining two resonances at 6.6 GeV.

The $I(J^P) = 0(2^+)$ sector: ωB_s^* and K^*B^* in both color-singlet and hidden-color channels, along with two diquark-antidiquark, and six K-type channels are considered in this case. First, the bound state is not found in single- and coupled-channel computations. The lowest-lying channel is the ωB_s^* scattering state. Additionally, other channels with exotic color structures are located in $6.36-6.52$ GeV. When a coupled-channel calculation is performed in each specific configuration, their lowest mass is ~ 6.4 GeV.

Furthermore, Fig. 10 presents results in the fully coupled-channel case using the CSM. Therein, scattering states of ωB_s^*, K^*B^*, and $\omega(1S)B_s^*(2S)$ are fully shown; additionally, four narrow resonances are also found. Table 21 presents their resonance parameters: $6239+\mathrm{i}0.8$, $6314+\mathrm{i}3.5$, $6619+\mathrm{i}4$, and $6664+\mathrm{i}6.9$ MeV, respectively. Moreover, the size of these four resonances is approximately 1.4 fm; the proportions of singlet-, hidden-color, diquark-antidiquark, and K-type channels are comparable. They can be further confirmed experimentally in

Table 18. Lowest-lying $\bar{q}q\bar{s}b$ tetraquark states with $I(J^P) = 0(1^+)$ calculated within the real range formulation of the chiral quark model. The results are presented in the same manner as that in Table 4 (unit: MeV).

Channel	Index	$\chi_J^{\sigma_i};\chi_I^{f_j};\chi_k^c$ $[i;j;k]$	M	Mixed
$(\eta B_s^*)^1(5963)$	1	[1; 1; 1]	6089	
$(\omega B_s)^1(6149)$	2	[2; 1; 1]	6051	
$(\omega B_s^*)^1(6197)$	3	[3; 1; 1]	6096	
$(KB^*)^1(5819)$	4	[1; 1; 1]	5800	
$(K^*B)^1(6172)$	5	[2; 1; 1]	6185	
$(K^*B^*)^1(6217)$	6	[3; 1; 1]	6226	5800
$(\eta B_s^*)^8$	7	[1; 1; 2]	6614	
$(\omega B_s)^8$	8	[2; 1; 2]	6496	
$(\omega B_s^*)^8$	9	[3; 1; 2]	6470	
$(KB^*)^8$	10	[1; 1; 2]	6361	
$(K^*B)^8$	11	[2; 1; 2]	6360	
$(K^*B^*)^8$	12	[3; 1; 2]	6497	6315
$(qb)(\bar{q}\bar{s})^*$	13	[4; 2; 4]	6498	
$(qb)(\bar{q}\bar{s})^*$	14	[4; 3; 3]	6239	
$(qb)^*(\bar{q}\bar{s})$	15	[5; 2; 3]	6474	
$(qb)^*(\bar{q}\bar{s})$	16	[5; 3; 4]	6473	
$(qb)^*(\bar{q}\bar{s})^*$	17	[6; 2; 3]	6466	
$(qb)^*(\bar{q}\bar{s})^*$	18	[6; 3; 4]	6421	6140
K_1	19	[7; 1; 5]	6480	
	20	[8; 1; 5]	6410	
	21	[9; 1; 5]	6588	
	22	[7; 1; 6]	6351	
	23	[8; 1; 6]	6352	
	24	[9; 1; 6]	6405	6299
K_2	25	[10; 1; 7]	6420	
	26	[11; 1; 7]	6502	
	27	[12; 1; 7]	6491	
	28	[10; 1; 8]	6353	
	29	[11; 1; 8]	6521	
	30	[12; 1; 8]	6512	6254
K_3	31	[13; 2; 10]	6389	
	32	[13; 3; 9]	6386	
	33	[14; 2; 10]	6488	
	34	[14; 3; 9]	6398	
	35	[15; 2; 10]	6474	
	36	[15; 3; 9]	6231	6063
Complete coupled-channels:				5800

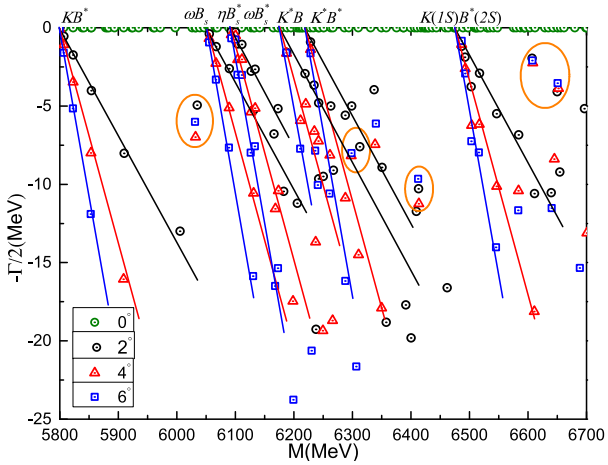

Fig. 9. (color online) Complete coupled-channel calculation of the $\bar{q}q\bar{s}b$ tetraquark system with $I(J^P) = 0(1^+)$ quantum numbers.

Table 19. Compositeness of exotic resonances obtained in a complete coupled-channel calculation in the $0(1^+)$ state of the $\bar{q}q\bar{s}b$ tetraquark. The results are presented in the same manner as that in Table 5.

Resonance	Structure
$6031+i12.0$	$r_{q\bar{q}}$: 1.85; $r_{\bar{q}\bar{q}}$: 1.87; $r_{b\bar{q}}$: 0.73; r_{qb} : 1.81
	S: 21.3%; H: 10.1%; Di: 16.6%; K: 52.0%
$6298+i16.0$	$r_{q\bar{q}}$: 1.95; $r_{\bar{q}\bar{q}}$: 1.94; $r_{b\bar{q}}$: 0.91; r_{qb} : 1.86
	S: 27.4%; H: 10.6%; Di: 10.2%; K: 51.8%
$6413+i20.6$	$r_{q\bar{q}}$: 1.22; $r_{\bar{q}\bar{q}}$: 1.55; $r_{b\bar{q}}$: 0.80; r_{qb} : 1.60
	S: 16.6%; H: 17.3%; Di: 21.9%; K: 44.2%
$6607+i4.2$	$r_{q\bar{q}}$: 1.56; $r_{\bar{q}\bar{q}}$: 1.84; $r_{b\bar{q}}$: 1.70; r_{qb} : 1.75
	S: 17.9%; H: 25.2%; Di: 12.6%; K: 44.3%
$6652+i7.7$	$r_{q\bar{q}}$: 1.61; $r_{\bar{q}\bar{q}}$: 1.93; $r_{b\bar{q}}$: 1.67; r_{qb} : 1.78
	S: 14.8%; H: 20.6%; Di: 27.4%; K: 37.2%

ωB_s^* and K^*B^* channels.

The $I(J^P) = 1(0^+)$ sector: First, all channels listed in Table 22 are investigated in the real-range computations, and no bound state is obtained. The lowest-lying scattering state is πB_s with a theoretical threshold value of 5504 MeV. The other three di-meson scattering states are ρB_s^*, KB, and K^*B^*. Furthermore, the masses of these four meson-meson structures in hidden-color channels are approximately 6.4 GeV; the values are similar for the K_1 channels, except for one at 5.79 GeV. For the diquark-antidiquark, K_2, and K_3 channels, they are generally located at 6.2 – 6.5 GeV. In coupled-channel studies, which include six partial and one complete channels calculations, strong and weak coupling effects are both presented. In particular, channel couplings in the hidden-color, diquark-antidiquark, K_2, and K_3 configurations are strong, and they exhibit 100 – 170 MeV mass shifts. Their low-

Table 20. Lowest-lying $\bar{q}q\bar{s}b$ tetraquark states with $I(J^P) = 0(2^+)$ calculated within the real range formulation of the chiral quark model. The results are presented in the same manner as that in Table 4 (unit: MeV).

Channel	Index	$\chi_J^{\sigma_i}; \chi_I^{f_j}; \chi_k^c$ $[i;j;k]$	M	Mixed
$(\omega B_s^*)^1(6197)$	1	[1; 1; 1]	6096	
$(K^*B^*)^1(6217)$	2	[1; 1; 1]	6226	6096
$(\omega B_s^*)^8$	3	[1; 1; 2]	6524	
$(K^*B^*)^8$	4	[1; 1; 2]	6497	6411
$(qb)^*(\bar{q}\bar{s})^*$	5	[1; 2; 3]	6422	
$(qb)^*(\bar{q}\bar{s})^*$	6	[1; 3; 4]	6435	6413
K_1	7	[1; 1; 5]	6489	
	8	[1; 1; 6]	6363	6362
K_2	9	[1; 1; 7]	6455	
	10	[1; 1; 8]	6458	6400
K_3	11	[1; 2; 10]	6403	
	12	[1; 3; 9]	6397	6387
Complete coupled-channels:				6096

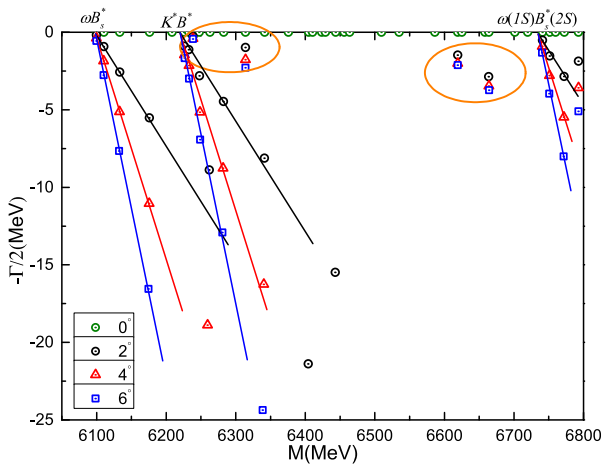

Fig. 10. (color online) Complete coupled-channel calculation of the $\bar{q}q\bar{s}b$ tetraquark system with $I(J^P) = 0(2^+)$ quantum numbers.

est masses are 6.24, 6.12, 6.20, and 6.03 GeV, respectively. However, the coupling is weak in color-singlet, K_1, and fully-coupled channels calculations. Accordingly, the scattering nature of πB_s remains unchanged.

In a further step, the complex-range study is conducted on the complete coupled-channel case. Six scattering states are plotted in Fig. 11, and they are the ground states of πB_s, KB, ρB_s^*, and K^*B^* and the first radial excitations of $\pi(1S)B_s(2S)$ and $K(1S)B(2S)$. Moreover, within an energy region of 5.5 – 6.5 GeV, two narrow resonance poles are obtained.

The compositeness of these resonances is listed in Table 23. First, the complex energies of the two reson-

Table 21. Compositeness of exotic resonances obtained in a complete coupled-channel calculation in the $0(2^+)$ state of the $\bar{q}q\bar{s}b$ tetraquark. The results are presented in the same manner as that in Table 5.

Resonance	Structure
$6239 + i0.8$	$r_{q\bar{q}}$: 1.45; $r_{\bar{q}\bar{q}}$: 1.50; $r_{b\bar{q}}$: 0.93; r_{qb} : 1.43
	S: 19.1%; H: 10.0%; Di: 12.8%; K: 58.1%
$6314 + i3.5$	$r_{q\bar{q}}$: 1.53; $r_{\bar{q}\bar{q}}$: 1.52; $r_{b\bar{q}}$: 0.80; r_{qb} : 1.44
	S: 22.4%; H: 6.4%; Di: 3.5%; K: 67.7%
$6619 + i4.0$	$r_{q\bar{q}}$: 1.42; $r_{\bar{q}\bar{q}}$: 1.44; $r_{b\bar{q}}$: 1.27; r_{qb} : 1.34
	S: 17.3%; H: 25.6%; Di: 14.0%; K: 43.1%
$6664 + i6.9$	$r_{q\bar{q}}$: 1.32; $r_{\bar{q}\bar{q}}$: 1.53; $r_{b\bar{q}}$: 1.34; r_{qb} : 1.41
	S: 12.1%; H: 18.0%; Di: 32.2%; K: 37.7%

Table 22. Lowest-lying $\bar{q}q\bar{s}b$ tetraquark states with $I(J^P) = 1(0^+)$ calculated within the real range formulation of the chiral quark model. The results are presented in the same manner as that in Table 4 (unit: MeV).

Channel	Index	$\chi_J^{\sigma_i}; \chi_I^{f_j}; \chi_k^c$ $[i;j;k]$	M	Mixed
$(\pi B_s)^1(5507)$	1	[1; 1; 1]	5504	
$(\rho B_s^*)^1(6185)$	2	[2; 1; 1]	6172	
$(KB)^1(5774)$	3	[1; 1; 1]	5759	
$(K^*B^*)^1(6217)$	4	[2; 1; 1]	6226	5504
$(\pi B_s)^8$	5	[1; 1; 2]	6494	
$(\rho B_s^*)^8$	6	[2; 1; 2]	6499	
$(KB)^8$	7	[1; 1; 2]	6361	
$(K^*B^*)^8$	8	[2; 1; 2]	6420	6243
$(qb)(\bar{q}\bar{s})$	9	[3; 2; 4]	6501	
$(qb)(\bar{q}\bar{s})$	10	[3; 3; 3]	6226	
$(qb)^*(\bar{q}\bar{s})^*$	11	[4; 2; 3]	6298	
$(qb)^*(\bar{q}\bar{s})^*$	12	[4; 3; 4]	6302	6123
K_1	13	[5; 1; 5]	6468	
	14	[6; 1; 5]	6463	
	15	[5; 1; 6]	6449	
	16	[6; 1; 6]	5792	5780
K_2	17	[7; 1; 7]	6315	
	18	[8; 1; 7]	6531	
	19	[7; 1; 8]	6417	
	20	[8; 1; 8]	6411	6200
K_3	21	[9; 2; 10]	6355	
	22	[9; 3; 9]	6203	
	23	[10; 2; 9]	6478	
	24	[10; 3; 10]	6221	6029
Complete coupled-channels:				5504

ances are expressed as $6080+\mathrm{i}2.5$ and $6149+\mathrm{i}1.6$ MeV, respectively. Meanwhile, they are compact $\bar{q}q\bar{s}b$ tetraquark structures, whose sizes are ~ 1.2 fm. The couplings among color-singlet, -octet, diquark-antidiquark, and K-type channels are strong. Both πB_s and KB are their golden channels to be discovered.

The $I(J^P)=1(1^+)$ sector: Table 24 lists 36 channels under consideration for this quantum state. In the meson-meson color-singlet channels, πB_s^*, $\rho B_s^{(*)}$, and $K^{(*)}B^{(*)}$ are calculated. The lowest channel is the scattering state of πB_s^*, and its mass is a theoretical threshold value of 5549 MeV. Moreover, the scattering nature of πB_s^* channel remains in partially and fully coupled-channel calculations. Other channels are also unbound. The channels in the other five structures, which are hidden-color, diquark-antidiquark, and K-types configurations, are generally located in an energy region of $6.2-6.5$ GeV, except for a K_1 channel at 5.8 GeV. Additionally, when coupled-channel calculations are considered in each of these five structures, a weak coupling effect is obtained in K_1 channels, and the lowest coupled mass is still 5.8 GeV. In contrast, strong coupling effects exist in other configurations. Nevertheless, they are still unstable excited states within $6.06-6.28$ GeV.

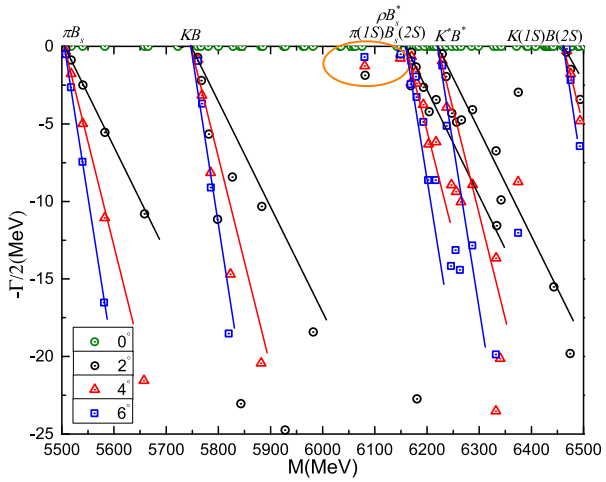

Fig. 11. (color online) Complete coupled-channel calculation of the $\bar{q}q\bar{s}b$ tetraquark system with $I(J^P)=1(0^+)$ quantum numbers.

Table 23. Compositeness of exotic resonances obtained in a complete coupled-channel calculation in the $1(0^+)$ state of the $\bar{q}q\bar{s}b$ tetraquark. The results are presented in the same manner as that in Table 5.

Resonance	Structure
$6080+\mathrm{i}2.5$	$r_{q\bar{q}}: 0.95$; $r_{\bar{q}\bar{q}}: 1.37$; $r_{b\bar{q}}: 1.24$; $r_{qb}: 1.27$
	S: 18.3%; H: 10.6%; Di: 12.8%; K: 58.3%
$6149+\mathrm{i}1.6$	$r_{q\bar{q}}: 1.09$; $r_{\bar{q}\bar{q}}: 1.13$; $r_{b\bar{q}}: 1.10$; $r_{qb}: 1.00$
	S: 18.5%; H: 10.5%; Di: 8.5%; K: 62.5%

Table 24. Lowest-lying $\bar{q}q\bar{s}b$ tetraquark states with $I(J^P)=1(1^+)$ calculated within the real range formulation of the chiral quark model. The results are presented in the same manner as that in Table 4 (unit: MeV).

Channel	Index	$\chi_J^{\sigma_i};\chi_I^{f_j};\chi_k^c$ $[i;j;k]$	M	Mixed
$(\pi B_s^*)^1(5555)$	1	[1; 1; 1]	5549	
$(\rho B_s)^1(6137)$	2	[2; 1; 1]	6127	
$(\rho B_s^*)^1(6185)$	3	[3; 1; 1]	6172	
$(KB^*)^1(5819)$	4	[1; 1; 1]	5800	
$(K^*B)^1(6172)$	5	[2; 1; 1]	6185	
$(K^*B^*)^1(6217)$	6	[3; 1; 1]	6226	5549
$(\pi B_s^*)^8$	7	[1; 1; 2]	6496	
$(\rho B_s)^8$	8	[2; 1; 2]	6550	
$(\rho B_s^*)^8$	9	[3; 1; 2]	6526	
$(KB^*)^8$	10	[1; 1; 2]	6361	
$(K^*B)^8$	11	[2; 1; 2]	6360	
$(K^*B^*)^8$	12	[3; 1; 2]	6460	6275
$(qb)(\bar{q}\bar{s})^*$	13	[4; 2; 4]	6498	
$(qb)(\bar{q}\bar{s})^*$	14	[4; 3; 3]	6239	
$(qb)^*(\bar{q}\bar{s})$	15	[5; 2; 3]	6474	
$(qb)^*(\bar{q}\bar{s})$	16	[5; 3; 4]	6473	
$(qb)^*(\bar{q}\bar{s})^*$	17	[6; 2; 3]	6415	
$(qb)^*(\bar{q}\bar{s})^*$	18	[6; 3; 4]	6370	6159
K_1	19	[7; 1; 5]	6536	
	20	[8; 1; 5]	6474	
	21	[9; 1; 5]	6466	
	22	[7; 1; 6]	6442	
	23	[8; 1; 6]	6443	
	24	[9; 1; 6]	5809	5800
K_2	25	[10; 1; 7]	6468	
	26	[11; 1; 7]	6405	
	27	[12; 1; 7]	6491	
	28	[10; 1; 8]	6415	
	29	[11; 1; 8]	6418	
	30	[12; 1; 8]	6512	6261
K_3	31	[13; 2; 10]	6454	
	32	[13; 3; 9]	6451	
	33	[14; 2; 10]	6358	
	34	[14; 3; 9]	6224	
	35	[15; 2; 10]	6474	
	36	[15; 3; 9]	6231	6065
Complete coupled-channels:				5549

In the complete coupled-channel computation using CSM, the distribution of complex energies is plotted in Fig. 12. Particularly, within an energy region of 5.55–6.45 GeV in the top panel of Fig. 12, the scattering states of πB_s^*, KB^*, ρB_s, and K^*B^* are well presented. Furthermore, dense distributions of energy dots occur at approximately 6.2 GeV; hence, an enlarged part from 6.12 to 6.22 GeV is plotted in the bottom panel. Therein, four scattering states of $\rho B_s^{(*)}$, K^*B, and $\pi(1S)B_s^*(2S)$ are shown.

In addition to the obtained continuum states, four resonances are found in complex plane. Table 25 summarizes their calculated results. First, the four stable poles are $5764+\mathrm{i}0.4$, $6103+\mathrm{i}10.3$, $6308+\mathrm{i}8.4$, and $6413+\mathrm{i}3.8$ MeV, respectively. Moreover, color-singlet, diquark-antidiquark, and K-type channels couplings are strong for the resonances. A compact structure, with a size of approximately 0.8 fm, is obtained for the lowest resonance at 5.76 GeV, and the dominant meson-meson component is πB_s^*. However, the other three resonances are loose structures with a size of ~ 1.6 fm. The golden channels of the second resonance at 6.1 GeV are πB_s^* and KB^*, whereas πB_s^*, K^*B, and K^*B^* channels are suggested to be the dominant di-meson components for the other two higher resonances at 6.3 and 6.4 GeV, respectively.

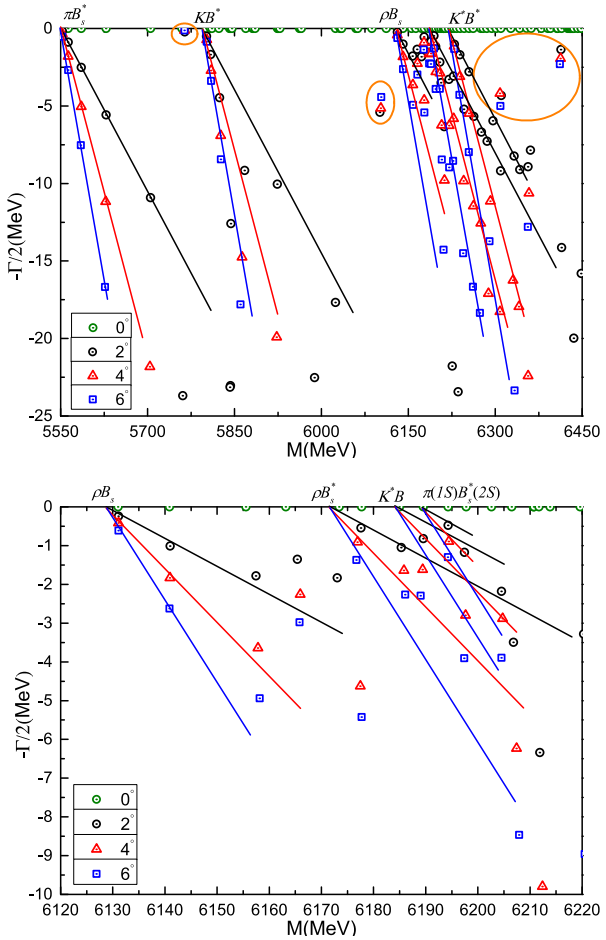

Fig. 12. (color online) *Top panel:* Complete coupled-channel calculation of the $\bar{q}q\bar{s}b$ tetraquark system with $I(J^P) = 1(1^+)$ quantum numbers. In particular, the bottom panel shows enlarged parts of dense energy region from 6.12 GeV to 6.22 GeV.

The $I(J^P) = 1(2^+)$ sector: Twelve channels listed in Table 26 are studied for the highest spin and isospin state of the $\bar{q}q\bar{s}b$ tetraquark. First, the bound states are not found in three types of calculations: single, partially coupled, and fully coupled-channels. The lowest scattering state is ρB_s^*, with a theoretical threshold value of 6172 MeV; another one is the 6226 MeV threshold value of the K^*B^* channel. Furthermore, the masses of channels in five exotic color structures are generally located in the energy region of 6.4 – 6.5 GeV. The lowest mass ob-

Table 25. Compositeness of exotic resonances obtained in a complete coupled-channel calculation in the $1(1^+)$ state of the $\bar{q}q\bar{s}b$ tetraquark. The results are presented in the same manner as that in Table 5.

Resonance	Structure
$5764+\mathrm{i}0.4$	$r_{q\bar{q}}$: 0.89; $r_{\bar{q}\bar{q}}$: 0.89; $r_{b\bar{q}}$: 0.78; r_{qb} : 0.69
	S: 29.6%; H: 2.4%; Di: 9.2%; K: 58.8%
$6103+\mathrm{i}10.3$	$r_{q\bar{q}}$: 0.93; $r_{\bar{q}\bar{q}}$: 1.73; $r_{b\bar{q}}$: 1.58; r_{qb} : 1.66
	S: 17.6%; H: 13.1%; Di: 23.2%; K: 46.1%
$6308+\mathrm{i}8.4$	$r_{q\bar{q}}$: 1.17; $r_{\bar{q}\bar{q}}$: 1.65; $r_{b\bar{q}}$: 1.40; r_{qb} : 1.37
	S: 11.4%; H: 6.1%; Di: 11.7%; K: 70.8%
$6413+\mathrm{i}3.8$	$r_{q\bar{q}}$: 1.50; $r_{\bar{q}\bar{q}}$: 1.63; $r_{b\bar{q}}$: 1.55; r_{qb} : 1.40
	S: 15.6%; H: 19.8%; Di: 27.3%; K: 37.3%

Table 26. Lowest-lying $\bar{q}q\bar{s}b$ tetraquark states with $I(J^P) = 1(2^+)$ calculated within the real range formulation of the chiral quark model. The results are presented in the same manner as that in Table 4 (unit: MeV).

Channel	Index	$\chi_J^{\sigma_i}; \chi_I^{f_j}; \chi_k^c$ $[i;j;k]$	M	Mixed
$(\rho B_s^*)^1(6185)$	1	[1; 1; 1]	6172	
$(K^*B^*)^1(6217)$	2	[1; 1; 1]	6226	6172
$(\rho B_s^*)^8$	3	[1; 1; 2]	6575	
$(K^*B^*)^8$	4	[1; 1; 2]	6531	6448
$(qb)^*(\bar{q}\bar{s})^*$	5	[1; 2; 3]	6472	
$(qb)^*(\bar{q}\bar{s})^*$	6	[1; 3; 4]	6479	6462
K_1	7	[1; 1; 5]	6544	
	8	[1; 1; 6]	6453	6452
K_2	9	[1; 1; 7]	6500	
	10	[1; 1; 8]	6510	6451
K_3	11	[1; 2; 10]	6466	
	12	[1; 3; 9]	6462	6452
Complete coupled-channels:				6172

tained within a coupled-channel calculation for each specific configuration is always located at ~ 6.45 GeV.

Figure 13 shows the distribution of complex energies in the complete coupled-channel computation using the CSM. Within the 6.15 – 6.80 GeV energy region, the ρB_s^* and K^*B^* scattering states are clearly presented. Meanwhile, four stable resonance poles are also obtained, and they are circled in the complex plane.

Table 27 lists the properties of these resonances. In particular, their complex energies are 6301 + i0.8, 6399 + i2.6, 6654 + i5.3, and 6740 + i10 MeV, respectively. The couplings among color-singlet, -octet, diquark-antidiquark, and *K*-type channels are strong for the first three resonances. However, only a strong coupling exists between diquark-antidiquark and *K*-type channels for the highest resonance. Moreover, the compact $\bar{q}q\bar{s}b$ tetraquark structure is obtained for the four resonances because their sizes are less than 1.5 fm. Finally, both ρB_s^* and K^*B^* are the dominant meson-meson components of these exotic states.

IV. SUMMARY

The *S*-wave $\bar{q}q\bar{s}Q$ ($q = u, d$; $Q = c, b$) tetraquarks with spin-parities of $J^P = 0^+$, 1^+, and 2^+ and isospins of $I = 0$ and 1 are systematically investigated under a chiral quark model formalism. Furthermore, the color-singlet, -octet meson-meson configurations, diquark-antidiquark arrangements with their allowed color triplet-antitriplet and sextet-antisextet channels, and K-type configurations are considered. The four-body bound and resonant states are determined using a highly efficient numerical approach: the Gaussian expansion method (GEM) supplemented with a complex-scaling analysis (CSM). Three types of computations are generally presented: single, partially-coupled, and fully-coupled channels.

Table 28 summarizes our theoretical findings for the $\bar{q}q\bar{s}c$ and $\bar{q}q\bar{s}b$ tetraquark systems. The first column shows the quantum numbers $I(J^P)$, the second one expresses the dominant configurations, and the third one lists the complex eigenenergies.

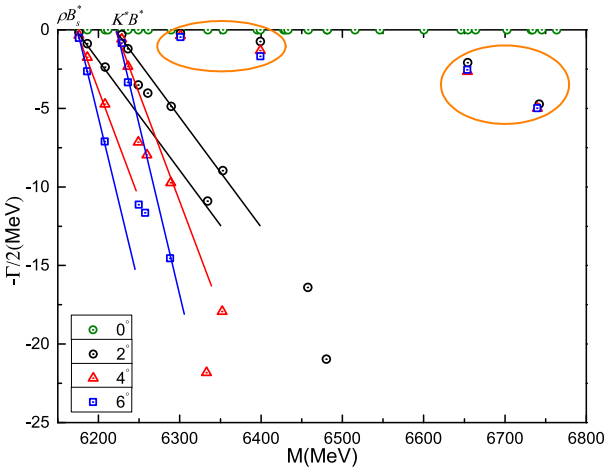

Fig. 13. (color online) Complete coupled-channel calculation of the $\bar{q}q\bar{s}b$ tetraquark system with $I(J^P) = 1(2^+)$ quantum numbers.

Table 27. Compositeness of exotic resonances obtained in a complete coupled-channel calculation in the $1(2^+)$ state of the $\bar{q}q\bar{s}b$ tetraquark. The results are presented in the same manner as that in Table 5.

Resonance	Structure
6301 + i0.8	$r_{q\bar{q}}$: 1.03; $r_{\bar{q}\bar{q}}$: 1.08; $r_{b\bar{q}}$: 0.95; r_{qb} : 1.00
	S: 15.1%; *H*: 11.5%; *Di*: 13.9%; *K*: 59.5%
6399 + i2.6	$r_{q\bar{q}}$: 1.16; $r_{\bar{q}\bar{q}}$: 1.14; $r_{b\bar{q}}$: 0.79; r_{qb} : 1.02
	S: 15.2%; *H*: 15.9%; *Di*: 11.8%; *K*: 57.1%
6654 + i5.3	$r_{q\bar{q}}$: 1.48; $r_{\bar{q}\bar{q}}$: 1.50; $r_{b\bar{q}}$: 1.34; r_{qb} : 1.43
	S: 10.4%; *H*: 15.4%; *Di*: 27.8%; *K*: 46.4%
6740 + i10.0	$r_{q\bar{q}}$: 1.48; $r_{\bar{q}\bar{q}}$: 1.42; $r_{b\bar{q}}$: 1.16; r_{qb} : 1.32
	S: 4.9%; *H*: 7.3%; *Di*: 41.6%; *K*: 46.2%

All identified exotic states are expected to be confirmed in future high-energy particle and nuclear experiments.

Table 28. Summary of resonance structures found in $\bar{q}q\bar{s}Q$ ($q = u, d$; $Q = c, b$) tetraquark systems. The first column shows the isospin, total spin, and parity of each singularity. The second column refers to the dominant configuration components; *H*: hidden color, *Di*: diquark-antidiquark, and *K*: *K*-type. Theoretical resonances are presented with the notation $E = M + i\Gamma$ in the last column (unit: MeV).

$\bar{q}q\bar{s}c$ tetraquarks		
$I(J^P)$	Dominant Component	Theoretical resonance
$0(0^+)$	$\omega D_s^*(10\%) + K^*D^*(11\%) + Di(13\%) + K(57\%)$	3006 + i6.3
$0(1^+)$	$H(19\%) + Di(30\%) + K(43\%)$	3119 + i19.8
	$Di(35\%) + K(42\%)$	3292 + i13.1
	$Di(35\%) + K(50\%)$	3346 + i22.0

Continued on next page

Table 28-continued from previous page

$0(2^+)$	$\omega D_s^*(12\%) + K^* D^*(7\%) + Di(28\%) + K(45\%)$	$2965 + i0.5$
	$\omega D_s^*(8\%) + K^* D^*(7\%) + H(13\%) + K(65\%)$	$3026 + i3.8$
	$H(20\%) + Di(19\%) + K(48\%)$	$3344 + i3.3$
$1(0^+)$	$H(19\%) + Di(30\%) + K(35\%)$	$2770 + i1.5$
$1(1^+)$	$\pi D_s^*(24\%) + Di(14\%) + K(56\%)$	$2470 + i1.0$
	$K^* D^*(10\%) + H(18\%) + Di(17\%) + K(49\%)$	$3134 + i2.0$
$1(2^+)$	$Di(27\%) + K(43\%)$	$3031 + i0.7$
	$H(22\%) + Di(28\%) + K(46\%)$	$3105 + i3.7$
	$Di(27\%) + K(55\%)$	$3373 + i4.2$
	$Di(39\%) + K(44\%)$	$3455 + i12.9$
	$\bar{q}q\bar{s}b$ tetraquarks	
$I(J^P)$	Dominant Component	Theoretical resonance
$0(0^+)$	$KB(17\%) + Di(14\%) + K(59\%)$	$6011 + i9.0$
	$K^* B^*(10\%) + Di(22\%) + K(54\%)$	$6323 + i4.0$
	$H(18\%) + Di(25\%) + K(49\%)$	$6397 + i13.8$
	$H(21\%) + Di(31\%) + K(34\%)$	$6643 + i23.4$
	$H(28\%) + Di(21\%) + K(33\%)$	$6678 + i16.0$
$0(1^+)$	$KB^*(17\%) + Di(17\%) + K(52\%)$	$6031 + i12.0$
	$K^* B(10\%) + K^* B^*(12\%) + K(52\%)$	$6298 + i16.0$
	$Di(22\%) + K(44\%)$	$6413 + i20.6$
	$KB^*(11\%) + H(25\%) + K(44\%)$	$6607 + i4.2$
	$H(21\%) + Di(27\%) + K(37\%)$	$6652 + i7.7$
$0(2^+)$	$\omega B_s^*(9\%) + K^* B^*(10\%) + Di(13\%) + K(58\%)$	$6239 + i0.8$
	$\omega B_s^*(15\%) + K^* B^*(7\%) + K(68\%)$	$6314 + i3.5$
	$\omega B_s^*(11\%) + K^* B^*(7\%) + H(26\%) + K(43\%)$	$6619 + i4.0$
	$H(18\%) + Di(32\%) + K(38\%)$	$6664 + i6.9$
$1(0^+)$	$\pi B_s(7\%) + KB(8\%) + Di(13\%) + K(58\%)$	$6080 + i2.5$
	$\pi B_s(8\%) + KB(5\%) + H(11\%) + K(63\%)$	$6149 + i1.6$
$1(1^+)$	$\pi B_s^*(27\%) + K(59\%)$	$5764 + i0.4$
	$Di(23\%) + K(46\%)$	$6103 + i10.3$
	$\pi B_s^*(4\%) + K^* B^*(5\%) + K(71\%)$	$6308 + i8.4$
	$\pi B_s^*(6\%) + K^* B^*(4\%) + Di(27\%) + K(37\%)$	$6413 + i3.8$
$1(2^+)$	$\rho B_s^*(6\%) + K^* B^*(9\%) + Di(14\%) + K(60\%)$	$6301 + i0.8$
	$\rho B_s^*(13\%) + H(16\%) + K(57\%)$	$6399 + i2.6$
	$Di(28\%) + K(46\%)$	$6654 + i5.3$
	$Di(42\%) + K(46\%)$	$6740 + i10.0$

References

[1] R. Aaij *et al*. (LHCb Collaboration), Phys. Rev. D **102**, 112003 (2020), arXiv:2009.00026[hep-ex]

[2] R. Aaij *et al*. (LHCb Collaboration), Phys. Rev. Lett. **125**, 242001 (2020), arXiv:2009.00025[hep-ex]

[3] R. Aaij *et al*. (LHCb Collaboration), Phys. Rev. Lett. **131**, 041902 (2023), arXiv:2212.02716[hep-ex]

[4] R. Aaij *et al*. (LHCb Collaboration), Phys. Rev. D **108**, 012017 (2023), arXiv:2212.02717[hep-ex]

[5] P. G. Ortega, D. R. Entem, F. Fernandez *et al*., arXiv: 2305.14430[hep-ph]

[6] M.-Y. Duan, M.-L. Du, Z.-H. Guo *et al*., Phys. Rev. D **108**, 074006 (2023), arXiv:2307.04092[hep-ph]

[7] B. Wang, K. Chen, L. Meng *et al.*, arXiv: 2309.02191[hep-ph]
[8] S. S. Agaev, K. Azizi, and H. Sundu, Phys. Rev. D **107**, 094019 (2023), arXiv:2212.12001[hep-ph]
[9] S. S. Agaev, K. Azizi, and H. Sundu, J. Phys. G **50**, 055002 (2023), arXiv:2207.02648[hep-ph]
[10] J. Wei, Y.-H. Wang, C.-S. An *et al.*, Phys. Rev. D **106**, 096023 (2022), arXiv:2210.04841[hep-ph]
[11] X.-S. Yang, Q. Xin, and Z.-G. Wang, Int. J. Mod. Phys. A **38**, 2350056 (2023), arXiv:2302.01718[hep-ph]
[12] R. Molina and E. Oset, Phys. Rev. D **107**, 056015 (2023), arXiv:2211.01302[hep-ph]
[13] H.-W. Ke, Y.-F. Shi, X.-H. Liu *et al.*, Phys. Rev. D **106**, 114032 (2022), arXiv:2210.06215[hep-ph]
[14] Z.-L. Yue, C.-J. Xiao, and D.-Y. Chen, Phys. Rev. D **107**, 034018 (2023), arXiv:2212.03018[hep-ph]
[15] Z.-L. Yue, C.-J. Xiao, and D.-Y. Chen, Eur. Phys. J. C **83**, 769 (2023), arXiv:2308.15355[hep-ph]
[16] D.-K. Lian, W. Chen, H.-X. Chen *et al.*, arXiv: 2302.01167[hep-ph]
[17] W.-T. Lyu, Y.-H. Lyu, M.-Y. Duan *et al.*, arXiv: 2306.16101[hep-ph]
[18] Y. Huang, H. Hei, J.-w. Feng *et al.*, arXiv: 2308.14148[hep-ph]
[19] M.-Y. Duan, E. Wang, and D.-Y. Chen, arXiv: 2305.09436[hep-ph]
[20] W.-T. Lyu, Y.-H. Lyu, M.-Y. Duan *et al.*, arXiv: 2310.11139[hep-ph]
[21] X.-K. Dong, F.-K. Guo, and B.-S. Zou, Phys. Rev. Lett. **126**, 152001 (2021), arXiv:2011.14517[hep-ph]
[22] H.-X. Chen, W. Chen, X. Liu *et al.*, Phys. Rept. **639**, 1 (2016), arXiv:1601.02092[hep-ph]
[23] H.-X. Chen, W. Chen, X. Liu *et al.*, Rept. Prog. Phys. **80**, 076201 (2017), arXiv:1609.08928[hep-ph]
[24] F.-K. Guo, C. Hanhart, U.-G. Meißner *et al.*, Rev. Mod. Phys. **90**, 015004 (2018), arXiv:1705.00141[hep-ph]
[25] Y.-R. Liu, H.-X. Chen, W. Chen *et al.*, Prog. Part. Nucl. Phys. **107**, 237 (2019), arXiv:1903.11976[hep-ph]
[26] G. Yang, J. Ping, and J. Segovia, Symmetry **12**, 1869 (2020), arXiv:2009.00238[hep-ph]
[27] X.-K. Dong, F.-K. Guo, and B.-S. Zou, Commun. Theor. Phys. **73**, 125201 (2021), arXiv:2108.02673[hep-ph]
[28] H.-X. Chen, Phys. Rev. D **105**, 094003 (2022), arXiv:2103.08586[hep-ph]
[29] X. Cao, arXiv: 2301.11253[hep-ph]
[30] M. Mai, U.-G. Meißner, and C. Urbach, Phys. Rept. **1001**, 1 (2023), arXiv:2206.01477[hep-ph]
[31] L. Meng, B. Wang, G.-J. Wang *et al.*, arXiv: 2204.08716[hep-ph]
[32] H.-X. Chen, W. Chen, X. Liu *et al.*, Rept. Prog. Phys. **86**, 026201 (2023), arXiv:2204.02649[hep-ph]
[33] F.-K. Guo, H. Peng, J.-J. Xie *et al.*, arXiv: 2203.07141[hep-ph]
[34] P. G. Ortega and D. R. Entem, Symmetry **13**, 279 (2021), arXiv:2012.10105[hep-ph]
[35] H. Huang, C. Deng, X. Liu *et al.*, Symmetry **15**, 1298 (2023)
[36] R. F. Lebed, arXiv: 2308.00781[hep-ph], arXiv:2308.00781[hep-ph]
[37] B.-S. Zou, Sci. Bull. **66**, 1258 (2021), arXiv:2103.15273[hep-ph]
[38] M.-L. Du, V. Baru, F.-K. Guo *et al.*, JHEP **08**, 157 (2021), arXiv:2102.07159[hep-ph]
[39] E. Hiyama, Y. Kino, and M. Kamimura, Prog. Part. Nucl. Phys. **51**, 223 (2003)
[40] G. Yang, J. Ping, and F. Wang, Phys. Rev. D **95**, 014010 (2017)
[41] G. Yang, J. Ping, and J. Segovia, Phys. Rev. D **99**, 014035 (2019), arXiv:1809.06193[hep-ph]
[42] G. Yang, J. Ping, and J. Segovia, Phys. Rev. D **101**, 014001 (2020), arXiv:1911.00215[hep-ph]
[43] G. Yang, J. Ping, and J. Segovia, Phys. Rev. D **102**, 054023 (2020), arXiv:2007.05190[hep-ph]
[44] G. Yang, J. Ping, and J. Segovia, Phys. Rev. D **101**, 074030 (2020), arXiv:2003.05253[hep-ph]
[45] G. Yang, J. Ping, and J. Segovia, Phys. Rev. D **103**, 074011 (2021), arXiv:2101.04933[hep-ph]
[46] G. Yang, J. Ping, and J. Segovia, Phys. Rev. D **104**, 094035 (2021), arXiv:2109.04311[hep-ph]
[47] G. Yang, J. Ping, and J. Segovia, Phys. Rev. D **106**, 014021 (2022), arXiv:2204.08556[hep-ph]
[48] G. Yang, J. Ping, and J. Segovia, Eur. Phys. J. C **83**, 772 (2023), arXiv:2303.15388[hep-ph]
[49] G. Yang, J. Ping, and J. Segovia, arXiv: 2311.01044 [hep-ph]
[50] M. D. Scadron, Phys. Rev. D **26**, 239 (1982)
[51] G. S. Bali, H. Neff, T. Duessel *et al.* (SESAM Collaboration), Phys. Rev. D **71**, 114513 (2005), arXiv:hep-lat/0505012[hep-lat]
[52] J. Segovia, D. R. Entem, F. Fernandez *et al.*, Int. J. Mod. Phys. E **22**, 1330026 (2013), arXiv:1309.6926[hep-ph]
[53] J. Segovia, D. R. Entem, and F. Fernandez, Phys. Lett. B **662**, 33 (2008)
[54] J. Segovia, D. R. Entem, and F. Fernandez, Phys. Rev. D **91**, 094020 (2015), arXiv:1502.03827[hep-ph]
[55] P. G. Ortega, J. Segovia, D. R. Entem *et al.*, Eur. Phys. J. C **80**, 223 (2020), arXiv:2001.08093[hepph]
[56] A. Valcarce, F. Fernandez, P. Gonzalez *et al.*, Phys. Lett. B **367**, 35 (1996), arXiv:nucl-th/9509009[nucl-th]
[57] G. Yang, J. Ping, and J. Segovia, Few Body Syst. **59**, 113 (2018), arXiv:1709.09315[hep-ph]
[58] G. Yang, J. Ping, P. G. Ortega *et al.*, Chin. Phys. C **44**, 023102 (2020), arXiv:1904.10166[hep-ph]
[59] J. Segovia, A. M. Yasser, D. R. Entem *et al.*, Phys. Rev. D **80**, 054017 (2009)
[60] J. Segovia, D. R. Entem, and F. Fernandez, Phys. Rev. D **83**, 114018 (2011)
[61] J. Segovia, C. Albertus, D. R. Entem *et al.*, Phys. Rev. D **84**, 094029 (2011), arXiv:1107.4248[hep-ph]
[62] P. G. Ortega, J. Segovia, D. R. Entem *et al.*, Phys. Rev. D **81**, 054023 (2010), arXiv:0907.3997[hepph]
[63] P. G. Ortega, J. Segovia, D. R. Entem *et al.*, Phys. Rev. D **95**, 034010 (2017), arXiv:1612.04826[hepph]
[64] P. G. Ortega, J. Segovia, D. R. Entem *et al.*, Phys. Rev. D **94**, 114018 (2016), arXiv:1608.01325[hepph]
[65] P. G. Ortega, J. Segovia, D. R. Entem *et al.*, Eur. Phys. J. C **79**, 78 (2019), arXiv:1808.00914[hep-ph]
[66] P. G. Ortega, J. Segovia, and F. Fernandez, Phys. Rev. D **104**, 094004 (2021), arXiv:2107.02544[hep-ph]
[67] P. G. Ortega, J. Segovia, D. R. Entem *et al.*, Phys. Lett. B **841**, 137918 (2023), arXiv:2211.06118[hepph]